A THESIS SUBMITTED TO
THE GRADUATE SCHOOL OF NATURAL AND APPLIED SCIENCES
OF ÇANKIRI KARATEKİN UNIVERSITY

SYNTHESIS AND CHARACTERIZATION OF SILVER NANOPARTICLES BY COLD PLASMA REACTION FOR BIOLOGICAL APPLICATIONS

IN PARTIAL FULFILLMENT OF THE REQUIREMENTS
FOR
THE DEGREE OF MASTER OF SCIENCE
IN
PHYSICS

BY

MURSHED HAMDAY JASEEM AL-JANABI

ÇANKIRI

2023

SYNTHESIS AND CHARACTERIZATION OF SILVER NANOPARTICLES BY COLD PLASMA REACTION FOR BIOLOGICAL APPLICATIONS

By Murshed Hamday Jaseem AL-JANABI

June 2023

We certify that we have read this thesis and that in our opinion it is fully adequate, in scope and in quality, as a thesis for the degree of Master of Science

Advisor **:** Prof. Dr. Çiğdem YÜKSEKTEPE ATAOL
Co-Advisor **:** Prof. Dr. Asmiet RAMIZY

Examining Committee Members:

Chairman **:** Prof. Dr. Çiğdem YÜKSEKTEPE ATAOL
Physics
Çankırı Karatekin University

Member **:** Prof. Dr. Sebahaddin ALPTEKİN
Physics
Çankırı Karatekin University

Member **:** Prof. Dr. Sibel DEMİR KANMAZALP
Technical Sciences, Biomedical Device Technology
Gaziantep University

Approved for the Graduate School of Natural and Applied Sciences

Prof. Dr. Hamit ALYAR
Director of Graduate School

I hereby declare that all information in this document has been obtained and presented in accordance with academic rules and ethical conduct. I also declare that, as required by these rules and conduct, I have fully cited and referenced all material and results that are not original to this work.

Murshed Hamday Jaseem AL-JANABI

ABSTRACT

SYNTHESIS AND CHARACTERIZATION OF SILVER NANOPARTICLES BY COLD PLASMA REACTION FOR BIOLOGICAL APPLICATIONS

Murshed Hamday Jaseem AL-JANABI

Master of Science in Physics

Advisor: Prof. Dr. Çiğdem YÜKSEKTEPE ATAOL

Co-Advisor: Prof. Dr. Asmiet RAMIZY

June 2023

Silver nanoparticles were synthesized by using cold atmospheric plasma which is generated by argon gas. The silver nanoparticles were prepared by using an aqueous solution of $AgNO_3$ with different concentrations (0.6, 0.8, 1, 1.2, and 1.4 mM) with an exposure time of 4 min. The UV-VIS spectrum for Ag nanoparticle solution exhibits peaks in the visible area between 416 and 433 nm, which demonstrates that Ag nanoparticle creation is caused by the surface Plasmon resonance. The concentration affects the peaks of the absorption spectra. Strong peaks can be seen in the XRD pattern of produced silver nanoparticles as a function of change in $AgNO_3$ concentration (0.6, 0.8, 1, 1.2, and 1.4 mM) with time. The particle size is variable and falls between the range of 30-74 nm, with a spherical form, according to the FESEM microscopic images of Ag nanoparticles of various concentrations at plasma exposure duration. Ag NPs at a concentration of 1 mM and a plasma exposure time of 4 min are more stabilizing and less agglomerative than other Ag NP concentrations, according to DLS and Zeta potential (ZP) results. The biological activity of the synthesized Ag NPs against some pathogenic bacterial species (*S. aureus*, *E. coli*) was investigated by the well diffusion method and MIC method and showed superior antibacterial activity in terms of the well diffusion method.

2023, 77 pages

Keywords: Cold plasma, *E. coli,* Nanoparticle, Silver

ÖZET

BİYOLOJİK UYGULAMALAR İÇİN SOĞUK PLAZMA REAKSİYONU İLE GÜMÜŞ NANOPARTİKÜLLERİN SENTEZİ VE KARAKTERİZASYONU

Murshed Hamday Jaseem AL-JANABI
Fizik, Yüksek Lisans
Tez Danışmanı: Prof. Dr. Çiğdem YÜKSEKTEPE ATAOL
Eş Danışman: Prof. Dr. Asmiet RAMIZY
Haziran 2023

Gümüş nanopartiküller, argon gazı tarafından üretilen soğuk atmosferik plazma kullanılarak sentezlendi. Gümüş nanopartiküller, 4 dakika maruz kalma süresi ile farklı konsantrasyonlarda (0,6, 0,8, 1, 1,2 ve 1,4 mM'lik) sulu $AgNO_3$ çözeltisi kullanılarak hazırlandı. Ag nanoparçacık çözeltisi 416 ve 433 nm arasındaki görünür alanda pikler sergilemektedir, bu da Ag nanoparçacık oluşumunun yüzey Plazmon rezonansından kaynaklandığını göstermektedir. Konsantrasyon, absorpsiyon spektrumlarının tepe noktalarını etkilemektedir. Üretilen gümüş nanopartiküllerin XRD deseninde $AgNO_3$ konsantrasyonundaki (0,6, 0,8, 1, 1,2 ve 1,4 mM) zamanla değişimin bir fonksiyonu olarak güçlü pikler görülebilir. Plazmaya maruz kalma süresinde çeşitli konsantrasyonlardaki Ag nanopartiküllerinin FESEM mikroskobik görüntülerine göre, partikül boyutu değişkendir ve küresel bir formla 30-74 nm aralığındadır. DLS ve Zeta potansiyeli (ZP) sonuçlarına göre, 1 mM konsantrasyondaki ve 4 dakikalık plazma maruziyet süresindeki Ag NP'ler, diğer Ag NP konsantrasyonlarına göre daha stabilize edici ve daha az aglomeratiftir. Sentezlenen Ag NP'lerin bazı patojenik bakteri türlerine (*S. aureus*, *E. coli*) karşı biyolojik aktivitesi kuyu difüzyon ve MIC yöntemi ile araştırılmış ve kuyu difüzyon yöntemi üstün antibakteriyel aktivite sergilemiştir.

2023, 77 sayfa

Anahtar Kelimeler: Soğuk plazma, *E. coli*, Nanopatikül, Gümüş

PREFACE AND ACKNOWLEDGEMENTS

I would like to thank my thesis advisor and co-advisor, Prof. Dr. Çiğdem YÜKSEKTEPE ATAOL and Prof. Dr. Asmiet RAMIZY for her patience, guidance and understanding.

Murshed Hamday Jaseem AL-JANABI

Çankırı-2023

CONTENTS

LIST OF SYMBOLS

I_A	Absorbed intensity
A	Absorbance value
Å	Angstrom value
k_B	Boltzman constant
Cs	Crystal size
°C	Degree celsius
eV	Electron volt
E_g	Energy gap
k	Extinction coefficient
ν	Frequency value
d_{hkl}	Interplaner distance
kV	Kilo-volt
L/min	Liter per minute
$M_{(hkl)}$	Miller indices
nm	Nanometer value
NPs	Nanoparticles
E_{ph}	Phonon energy
λD	Plasma debye length
R	Reflectance value
I_R	Reflected intensity
K	Shape factor
I_o	Standard intensity

LIST OF ABBREVIATIONS

APPJ	Atmospheric pressure plasma jet
DBD	Dielectric barrier discharge
DLS	Dynamic light scattering
EDS	Energy dispersive X-ray spectroscopy
E. coli	*Escherichia coli*
FCC	Face center cubic
FESEM	Field emission scanning electron microscope
β (FWHM)	Full width at half maximum
ICP-MS	Inductively coupled plasma mass spectroscopy
PDI	Polydispersity index
PSD	Particle size distribution
Ag NPs	Silver nanoparticles
$AgNO_3$	Silver nitrate salt
S. aureus	*Staphylococcus aureus*
SPR	Surface plasmon resonance
UV-VIS	Ultraviolet-visible
XRD	X-ray diffraction
ZP	Zeta potential

LIST OF FIGURES

LIST OF TABLES

1. INTRODUCTION

Nanotechnology is the study of how to manipulate matter at the atomic or molecular level. A particle is referred to as a "nanoparticle" if all three dimensions are scaled in nanometers and it has a tiny number of atoms or component molecules that have different characteristics from their bulk counterparts and may take on different shapes. Material having at least one dimension and a size range of 1–100 nanometers is processed in this way. forms such as spherical, triangular, cubic, pentagonal, rod-shaped, shell-shaped, and elliptical (Kattumuri 2006). Several studies have asserted that tiny particles may be more damaging than larger ones since they have a larger surface area. Silver nanoparticles have a variety of potential applications in the domains of physics, chemistry, and biology. For quantitative measurement of electrical, magnetic, and other characteristics, it may act as a model system. As they vary from bulk materials in terms of their physical, biological, and chemical properties and have a bigger surface area per unit of weight or volume than larger particles, nanoscale particles are quite different from one another (He *et al.* 2013).

The antibacterial properties of silver have been well-known since water was first stored in silver vessels from 1000 B.C. The prevention of ocular infection in newborns is mentioned in the earliest scientific articles documenting the medicinal use of silver in 1881, and internal antisepsis is mentioned in 1901. Since then, warts have been removed and superficial and deep cutaneous burns or wounds treated with silver nitrate and silver sulfadiazine, respectively (Ayala-Núñez *et al.* 2009). Silver was used to treat bacterial infections less often after penicillin was created in the 1940s. Silver reappeared in the 1960s when Moyer suggested using 0.5% silver nitrate for the treatment of burns. Due to the rise in bacteria that are resistant to antibiotics and the limitations placed on their usage, doctors have recently returned to using silver wound dressings with varying amounts of silver. The powerful bactericidal and inhibitory properties of silver and its compounds, as well as a variety of antimicrobial activities for bacteria, fungi, and viruses, have been known since ancient times. Silver is more toxic to bacteria than other metals, but less toxic to human cells (Silver 2003). Silver nanoparticles have long been known, but little attention has been devoted to them, when compared to the noble metal's bulk form. Silver

shows a range of catalytic properties at the nanometric scale (less than 100 nm), including surface Plasmon resonance, a huge effective scattering cross section of individual silver nanoparticles, and severe toxicity to several microorganisms (Ayala-Núñez *et al.* 2009). The usage of silver nanoparticles (SNPs) for antibacterial applications seems to be reviving thanks to studies on metal nanoparticles. It has been demonstrated that SNPs created using various synthetic techniques have potent antibacterial action (Silver 2003).

Due to their compact size, nanoparticles have the highest activity to weight ratios since their entire surface area is maximized. Because of this substantial difference between this feature and the bulk metal, silver nanoparticles have gained a lot of interest and found use in a variety of fields, In various industrial, medical, and environmental domains, silver nanoparticles are used as filters to purify the air and water. Furthermore, biological techniques can be used to create nanosilver particles. Due to their strong response, the resulting nanoparticles have several uses as antibacterials and solar energy detector receptors. Due to their sensitivity, silver nanoparticles have several uses in the field of bimolecular detection. Despite the silver nanoparticles' slight toxicity to humans, it can be employed in diagnostic and therapeutic procedures because of its distinguishing trait; includes catalysis, textile engineering, biotechnology, optics, electronics, water treatment, and medicine. Nowadays, a variety of consumer goods, such as wet wipes, detergent, soap, shampoo, toothpaste, air filters, coatings for refrigerators, vacuum cleaners, washing machines, food storage containers, and mobile phones, as well as air freshener sprays, socks, pillows, slippers, and respirators, widely use silver nanoparticles as antibacterial/antifungal agents (Shrivastava *et al.* 2007, Buzea *et al.* 2007).

The aim of this study;

- Synthesis and study (Ag) nanoparticles on different substrates by cold plasma technique as a function of the plasma parameter
- Using Ag nanostructures to synthesize Nano-thin film using the Drop Casting method
- Examine the optical structural and morphological characteristics of thin films
- Determine the optimum conditions for Ag nanoparticles antibacterial application

2. LITERATURE REVIEW

Maria *et al.* (2010) used a simple way to introduce a considerable amount of silver nanoparticles into bacterial cellulose (BC) and then manufactured and studied the impregnation of those particles in that material. The nonporous colloidal structure works well as a nano reactor. Since silver particles are meant to be attached to the BC membrane, gelatin in particular works as a protector and is essential in avoiding the aggregation of silver particles and controlling their size. They claimed that the silver nanoparticles produced when hydroxylamine colloid was combined with the Ag composite based on bacterial cellulose were responsible for the Ag composite's potent bacterial activity.

Kim *et al.* (2011) aimed to produce silver nanoparticles and investigate their antibacterial activity. The silver ion was chemically reduced by ethanol in the presence of sodium linoleate. The growth inhibitors against *Staphylococcus bacillus*, *Staphylococcus aureus*, and *Pseudomonas aureginosa* were distributed uniformly, as demonstrated by the TEM method. They conclude that nanoparticles can be used to successfully inhibit the growth of certain bacteria.

According to Mahmood (2012), the creation of the AgNPs required the use of a PLA, a silver plate dipped in double-distilled water (DDW), and a 1064 nm Nd: YAG laser. When employing the AgNPs with amoxicillin and penicillin to explore how the disk diffusion mechanism affects the bacterial activity of different four prevalent antibiotics against gram-positive and gram-negative isolates Ceftriaxone and chloramphenicol are combined with AgNPs for the treatment of Gram-positive isolates.

Abdul-Hassan *et al.* (2018) used pulsed laser ablation of pure silver metal plates immersed in deionized and distilled water in the energy range of 100 to 400 mJ to form silver nanoparticles. The created nanoparticles are studied and assessed using a UV-VIS spectrophotometer and transmittance electron microscopy (TEM). The correlation between laser pulse energy and pulse count revealed that AgNPs inhibit bacterial growth. The silver nanoparticles showed a surface Plasmon resonance effect at a wavelength of

400 nm. Pure, spherical silver with a typical size of 1 to 15 nm was produced by them. Each size measurement has been validated by the TEM.

Kadhim Al-Ogaili *et al.* (2015) investigated the optical and antibacterial properties of silver nanoparticles formed by pulsed (Q-switched, 1064 and 532 nm dual frequency-Nd:YAG) laser ablation of silver metal in double distilled and deionized water (DDDW) using various methods. The influence of laser parameters, such as the number of pulses and laser intensity, was clarified in relation to nanoparticle features. It may be seen that the number and strength of laser pulses regulate the size of the nanoparticles. The average size of the created nanoparticles decreases with increasing laser energy and the number of pulses, as evidenced by the absorption peak of the nanoparticles showing a pronounced blue shift. The average size of the created nanoparticles decreases with increasing laser energy and the number of pulses, as evidenced by the absorption peak of the nanoparticles showing a pronounced blue shift. While ablating for a longer duration, the average size of nanoparticles decreases. Researchers tested the pathogens streptococcus, staphylococcus, proteus, and enterobacter to see if created silver nanoparticles had any antibacterial characteristics. Throughout the entire pulses, the solution's 400 nm absorbance measured with a 1064 nm laser was lower than the 400 nm absorbance obtained with a 532 nm laser. Contrary to the ablation efficiencies that have been reported, this predicts that the inter-pulse self-absorption efficiency for the 1064 nm laser should be lower than that for the 532 nm laser.

Silver nanoparticles of various sizes and shapes were injected via solution using a reduction method routing methodology. He employed sodium borohydride and trisodium citrate as reducing agents, as well as the silver nitrate that was added to a precursor. The morphology, shape, size, and structural characteristics of the obtained (PVP) SEM, UV-vis, and X-ray methods are rummage-sale, respectively, to describe nanoparticles. Noticed the spherical-shape of AgNPs and discovered that the width of particles ranged from 15 to 90 nm while the length of the particle was 150 nm. Additionally, it was discovered that different AgNPs' absorption peaks at wavelengths between 397 and 504 nm revealed When compared to the triangular and bigger spherical shaped AgNPs, the

lowest spherical size of AgNPs exhibited a high efficacy against bacterial strains (Raza *et al.* 2016).

According to Noori (2017), 200 pulses at two different laser energies (100 and 600 mJ) were required for the production of Ag nanoparticles from Ag metal in distilled water. The structural characteristics of the nanoparticles and the rate at which two different kinds of bacterial particles (*Staphylococcus aureus* and *E. coli*) were destroyed were then evaluated in relation to the preparation parameters. To efficiently prepare the nanoparticle to destroy the bacterium is the goal. Silver nanoparticles were created using a pulse laser with 100 mJ and 600 mJ for 400 and 4000 pulses, respectively. According to the findings of X-ray diffraction for the produced nanoparticles, the samples have a small crystalline size (about 9.8 nm). The resulting nanoparticles, as seen in the SEM image, varied in size from too small (less than 50 nm) to spherical. These samples were successful in the testing and shown to be efficient against the two bacterial species. While the energy was smaller (100 mJ), 200 pulses were used to prepare high-efficiency tests for the death of the samples; however, the 200 pulses used to produce the samples with high energy (600 mJ) were less successful. The bond (1611, 675) cm^{-1} for AgO is verified by FTIR spectra. Antibacterial activity studies performed on a variety of microorganisms clearly shown the effectiveness of nanoparticles against bacterial growth due to the smaller particle size that may penetrate the membrane of bacterial cells.

Al-Azawi *et al.* (2018) saw the use of the sol-gel method to create Ag-SiO_2 nanoparticles. The crystal structure of the nanocomposite was studied by X-ray diffraction patterns, and the colour intensity was determined by spectrophotometry. The range of average grain sizes for all samples, according to an AFM investigation of the morphology, was between 68.96 and 75.81 nm. Using scanning electron microscopy, Ag-SiO_2 nanoparticles were examined (SEM). Ag-SiO_2 NPs, which are very stable, have a considerable effect on both Gram-positive and -negative bacteria. *Staphylococcus aureus* and *Escherichia coli*, two pathogens, were used.the nanocomposite's antibacterial capabilities were evaluated. The findings indicated that Ag-SiO_2 produced as nanopowder and nanogel have antibacterial properties, with the Ag-SiO_2 nanopowder demonstrating the greatest antibacterial activity against *S. aureus*. Ag-SiO_2 NPs were inhibited by both biofilm preparation techniques,

however the synthetic Ag-SiO_2 NPs had the greatest inhibitory impact on the Gram-positive bacterium *S. aureus* when tested using the biofilm microtiter method.

Rheima *et al.* (2019) describes a novel UV-irradiation-based process for producing silver nanoparticles. X-ray diffraction, transmission electron spectroscopy, and a UV-visible spectrometer were used to describe the nanostructures. Ag NPs are primarily hexagonal in form, however some of them can also be spherical. The computed average size of nanoparticles was 20.23 nm. The ion concentration of the generated Ag NPs determines their shape, size, and UV absorbance and transmission. Because of their antibacterial action, silver nanoparticles, which have well-known antimicrobial properties become increasingly significant. As a result, their produced Ag NPs were effective against Gram-positive bacteria including *Staphylococcus aureus* and *E. coli* (Gram-negative bacteria). The results demonstrated that nanoparticles at 0.2 mg/mL concentration exhibited high antibacterial activity, which resulted in efficient suppression of both Gram-positive and Gram-negative bacteria. Yet, Ag NPs have a greater impact on gram-positive bacteria than gram-negative bacteria.

Vorobyova and Skiba (2021), investigated the stability of silver nanodispersions produced by a transient polyvinyl alcohol plasma discharge (PVA). On the creation of nanoparticles and their characteristics, the effects of crucial technical factors including initial Ag+ concentration, PVA concentration, and process length were examined (size and stability). The localized surface plasmon resonance was observed in UV-Vis spectra between 400 and 420 nm. SEM images show that Ag NPs have a spherical shape and an average particle size of up to 30 nm. Using Ag NPs as a catalyst, 4-Nitrophenol was decreased (4-NP). UV-Vis spectrophotometry is used to The effects of PNP concentration and catalyst dose on the apparent rate constant (kapp) for the catalytic reduction of 4-NP in the presence of Ag NPs was examined. They looked at the antibacterial effectiveness of Ag nanoparticles against yeast and *E. coli*. In colorimetric sensor tests, Ag NPs created in plasma demonstrated selective detection of the potentially harmful Hg^{+2} ion in water.

This chapter explained the plasma concept and the technical atmospheric-pressure plasma jet system characteristics are discussed. The main concepts of nanoparticles and (Ag NPs)

that rummage-sale in this research, and their wide range applications of for biological purposes. The theoretical framework of the prepared devices is discussed in this work. The effects of nanoparticles with unique properties on some bacterial species have been studied.

2.1 Silver Nitrate ($AgNO_3$)

Silver-Nitrate with its solid state is an inorganic compound, without color or very light color, crystal shape, turning to raven if exposed to lighting or organic matter. Its formulation of chemistry is $AgNO_3$. It contains an ionic bond among both the silver-cation (Ag^+) as well as a niter ion (NO_3^-) as shown in Figure 2.1. A trigonal planar configuration is coordinated with the silver nitrate. It is sometimes used as a prelude to many other combinations, which contain silver. Silver nitrate melting in water, so, it is regarded as one of the farthest remarkable salts of silver. It has been used in manufacturing films of photo-graphic, also in labs regulation as a staining factor in protein fantasy in PAGE gels, and in microscopy of scanning electrons, it can be used as a press or sclerosing factor, as well as an antiseptic impact (Liau *et al.* 1997). In this research, silver nitrate was used to obtain silver nanoparticles.

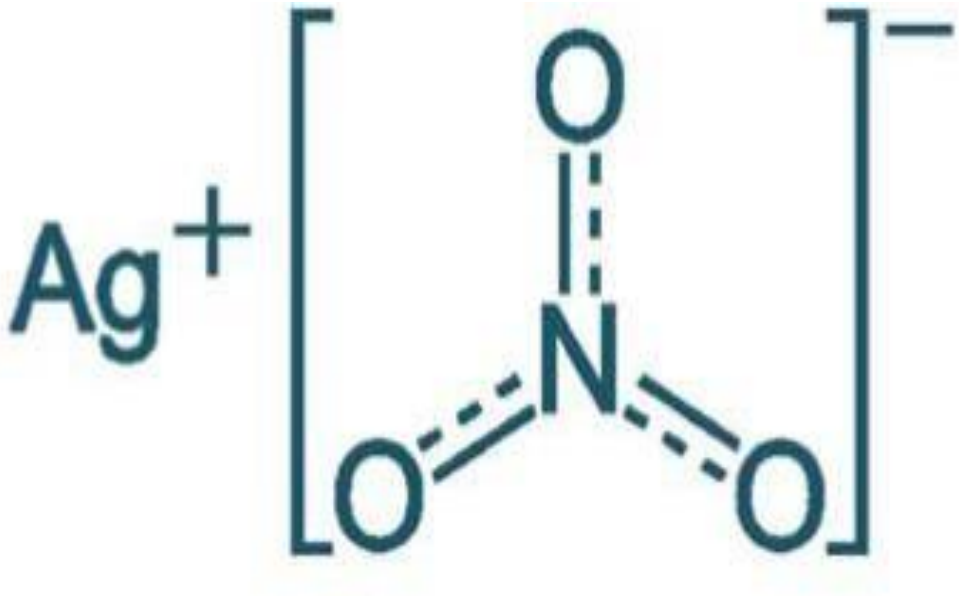

Figure 2.1 Chemical structure of silver nitrate ($AgNO_3$) (Liau *et al.* 1997)

The physical characteristics of silver nitrate are listed in Table 2.1 (Lide 2004).

Table 2.1 The thermal characteristic of silver nitrate ($AgNO_3$)

Characterizations	**Metric**
Density	4.35 g/cm^3
Molar mass	169.88 g/mol
Melting Point	210℃
Decomposed into silver	440℃
Boiling point	444℃

2.2 Silver Nanoparticles (Ag Nps)

Several physical, chemical, and biological processes can produce silver nanoparticles. Due to their distinctive qualities, based on optical, electrical, and magnetic characteristics, for example, silver nanoparticles are significant because they can be used in cryogenic superconducting materials, cryogenic antimicrobial treatment, biosensor materials, composite fibers (Šileikaitė *et al.* 2006). The metal nanoparticles, for example, the characteristic of SPR for Au and Ag affects both linear and nonlinear optical characteristics when metal nanoparticles are exposed to light. The physical properties of the metal fraction in a host matrix, such as silica, dictate the features of SPR. As is well knowledge, pure silver has greater thermal and electrical conductivity than the majority of metals and alloys. Nanosilver may enter cells and the body through a variety of entrance points due to its diverse applications (Scalisi *et al.* 2004).

Before the invention of chemical antibiotics, silver was employed since it had long been recognized to have antibacterial properties. In the presence of moisture, bodily fluids, and mucus, metallic silver, and the most inorganic silver compounds ionize to produce biologically active silver ions (Ag+), which are utilized as antibacterial agents. As they have potent antibacterial properties, silver nanoparticles (AgNPs) are often employed in industrial, everyday, and health-related goods (Sadeghi *et al.* 2010).

2.3 Synthesis of Ag Nps

Due to the many uses of nanotechnology at this time, the production of nanoparticles has become so important. Ag NPs are often synthesized using top-down and bottom-up techniques, as shown in Figure 2.2 (A). Whereas the top-down approach disincorporates bulk materials to obtain the required nanostructures, the bottom-up approach assembles single atoms and molecules into larger nanostructures to make nano-sized materials. Many physical, chemical, and biological processes may produce silver nanoparticles, as shown in Figure 2.2 (B), (C), and (D) (Skiba *et al.* 2018).

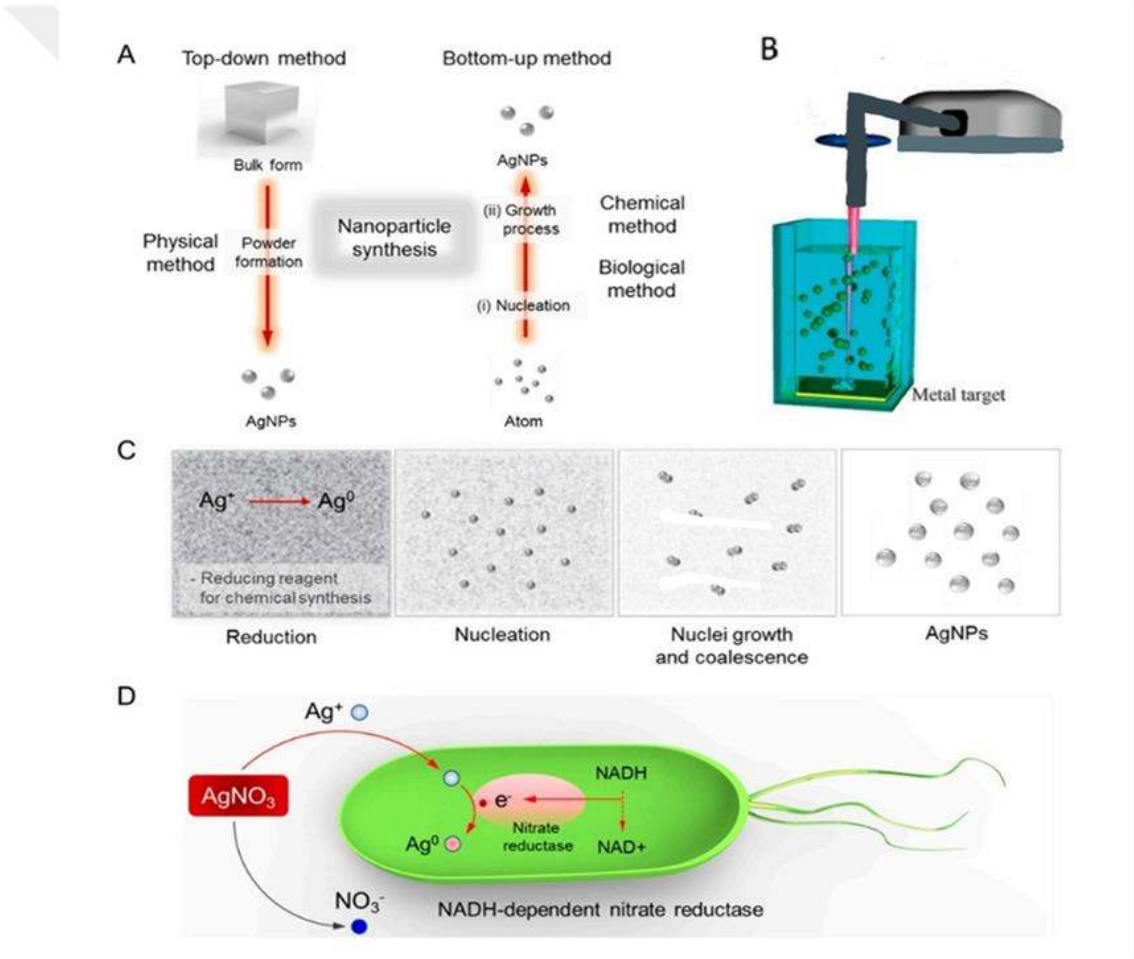

Figure 2.2 Several processes can be used to create silver nanoparticles (A) Bottom-up and top-down approaches (B) Physical synthesis technique (C) The use of chemical synthesis (D) Probable green chemistry synthesis methods (Skiba *et al.* 2018)

Contact non-equilibrium low-temperature plasma is a realistic option among plasma-chemical discharges from the standpoint of practical use. A plasma discharge takes place between the electrode in the gaseous phase and the other electrode, which is on the surface of the liquid. As a result, chemical changes at the phase interface are influenced by the combined impacts of electrochemical oxidation-reduction, initiated photolysis processes, UV radiation, and the passage of charged particles from the gaseous phase to the surface of the liquid medium. To some extent, the routes of chemical reactions and the makeup of the resulting products may be controlled by altering the composition of liquid phases. Prior studies have shown the efficiency of the contact non-equilibrium low-temperature plasma approach when compared to the conventional methods of chemical reduction in solutions and photochemical deposition. Water or an organic solvent are often employed as solvents in chemical operations to produce nanoparticles of silver or gold. A silver salt ($AgNO_3$) dissolved in water may be chemically reduced to create silver nanoparticles (Ag NPs) using reducing agents such as sodium borohydride ($NaBH_4$), citrate, glucose, hydrazine, and ascorbate. In the case of the two-stage reduction of silver, the first step is nucleation, followed by growth (Pivovarov *et al.* 2017, Skiba *et al.* 2017).

By adding a reducing agent and allowing silver atoms to form in solutions containing Ag+, AgNPs are commonly created. AgNPs are created when the silver atoms coagulate. Silver ions have been reduced using a variety of chemical and physical techniques. Plasmas can produce AgNPs without any negative byproducts and can decrease silver ions. In these experiments, a surfactant/stabilizer like fructose is frequently utilized to stop unchecked particle development and agglomeration. According to a recent study, gold nanoparticles may be electrostatically stabilized, even though AgNPs are stabilized by polymers or surfactants (Kondeti *et al.* 2017).

2.4 Plasma Overview

The Greek word "plasma," which means "jelly" or "moldable material," is the source of the name. and it was first used by chemist Irving Langmuir to describe the activity of ionized atomic nuclei and the electrons in the immediate vicinity. Figure 2.3 depicts the

four states of matter: solids, liquids, gases, and plasma. Solids, liquids, and gases are the other three (Burm 2012).

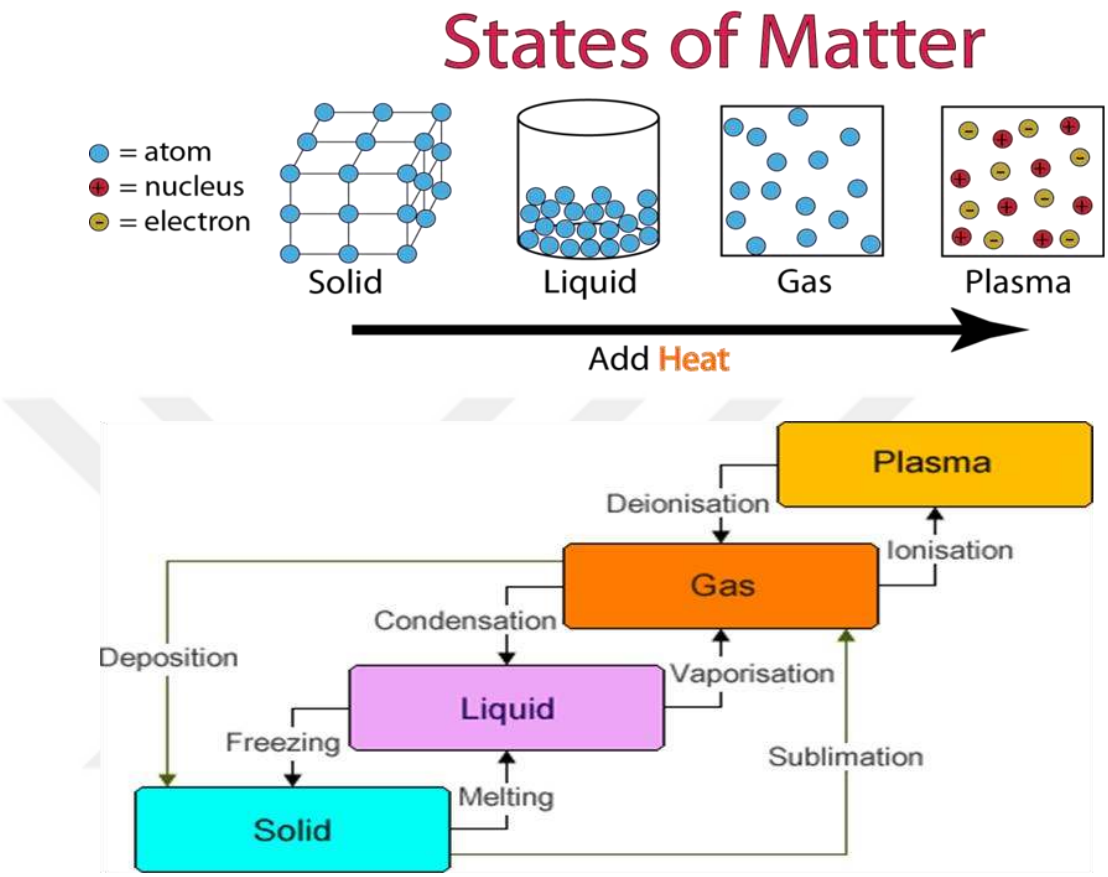

Figure 2.3 States of matter (Burm 2012)

Depending on plasma density and temperature, it can exhibit the characteristic of the behavior of the three familiar states. Plasma appears in space and astrophysics, laser-matter interaction, fusion, etc. By giving a gas particle energy to produce charged species, plasma is created. A significant quantity of energy is transformed into positive and negative charged particles; this energy is quickly used before it dissipates into the environment, and it is preserved to sustain the plasma state. This indicates that plasma is an ionized gas made up of neutral atoms or molecules mixing with free electrons, positive ions, and positive ions (Penache 2002).

2.4.1 Properties of plasma

- Since plasma is made up of charged particles, it is not as free as gas and carries electricity and electromagnetic forces. On the other hand, most gases act as electrical insulators.
- Plasma has no defined shape or volume.
- Layers, filaments, and beams can all be assumed if plasma is exposed to a magnetic field. Several of these structures may be seen in a plasma ball as a clear illustration.
- In general, plasma is much less pressurized than gas.
- Frequently resulting in the plasma maintaining a general shape or flow. The presence of charged particles also implies that plasma may be shaped or contained by electric and magnetic fields (Von Woedtke *et al.* 2019).

2.4.2 Plasma generation

Plasma occurs naturally or artificially, some examples of natural plasma are solar corona, lightning, and ionosphere. Artificial plasma is employed by semiconductors, lighting, synthetic fabrics treatment, plasma televisions, etc (Abdul-Hassan *et al.* 2018). Energy is applied to a neutral gas to create artificial plasma by triggering the creation of charge carriers in the gas. When sufficiently energetic electrons or photons strike neutral atoms and molecules in the feed gas, they combine to generate electrons and ions in the gas phase (electron-impact ionization or photoionization). The energy required for the neutral gas to become plasma may be delivered in several ways. Providing thermal energy, such as via fires, is one alternative (Söderström 2008). The most widely used method for producing and sustaining a low-temperature plasma for use in technological and technical applications involves applying an electric field to neutral gas. In every volume of a neutral gas, a few produced electrons and ions are constantly present. By adding energy to a gas, which causes some of its electrons to leave its atoms, plasma is produced. Ionization is the term used for this. As a consequence, electrons pick up a negative charge, and ions become positively charged, when exposed to electrical fields, charged particles in plasma will react more violently than charged particles in other states of matter. If plasma is not heated, ions will revert to their gaseous state and dissipate the energy that first ionized

them. A gas can be heated until it gets ionized or subjected to a strong electromagnetic field to form plasma, which is made up of positive ions and free electrons. An electric field accelerates the free charge carriers, and when they hit with gas atoms and molecules or the electrode surfaces, additional charged particles are correctly formed (Oberman 1965, Von Woedtke *et al.* 2019). An atmospheric pressure plasma jet was used in this study to create plasma.

2.4.3 Classifying plasma

There are many types of plasma (high-temperature plasma and low-temperature plasma). Thermal plasmas are those in which the temperature of the ions and the temperature of the electrons are equal. Nevertheless, non-thermal plasmas are those in which the temperature of the electrons is greater than that of the ions (Pekárek 2003, Söderström 2008).

2.4.3.1 Thermal plasma (tp)

In a thermal plasma, also referred to as an equilibrium plasma, all species (electron, ion, and neutral species) are in a state of thermal equilibrium. They often have petrol temperatures over 10.000 K. For instance, this equilibrium plasma must form at high temperatures, often between 4.000 K and 20.000 K, as seen in stars and fusion plasmas (Pekárek 2003).

2.4.3.2 Non-thermal plasma (ntp)

Non-thermal plasma is subdivided into quasi-equilibrium plasma, and no equilibrium plasma or cold plasma (Pekárek 2003).

Quasi-equilibrium plasma; Quasi-equilibrium plasmas, which show the temperatures of each plasma component in a local thermal equilibrium (LTE) condition are the same in localized areas in the plasma. Plasma torches and other thermal plasma sources are

frequently used in processes that require a high flow of heat, such as cutting, spraying, and welding (Nehra *et al.* 2008). Plasma is used for both material processing and waste material treatment. Even the most resistant wastes, such as toxic, medicinal, biohazardous, industrial, and nuclear waste, may be processed at high temperatures of quasi-equilibrium into elemental form, eventually lessening the environmental pollution they cause. Yet, the high-temperature property of quasi-equilibrium plasma is neither necessary nor desirable for several technological applications, and sometimes it even escalates in price. Cold plasmas are more appropriate in certain application sectors (Heberlein 2002).

Cold plasma; Different energy levels between electrons, ions, and neutral molecules define cold plasma, where electron temperatures can be 100 to 1000 times higher than neutral gas temperatures (Nehra *et al.* 2008). Such plasma is generated from electrical energy, where the plasma's electron component receives the most of the electrical energy, instead of heating the whole gas stream, energetic electrons are produced, keeping the plasma's ions and neutrals at or near room temperature (Fridman *et al.* 2005). Because the ions and the neutrals stay relatively cold, these energizing electrons ionize and split background molecules, producing chemical entities that are exceedingly reactive (radicals, ions, stimulated molecules). This quality makes it possible to treat materials that are sensitive to heat, such as polymers and biological tissue, utilizing cold plasmas. Due to the extraordinary characteristics of cold plasma, which include a strong thermodynamic non-equilibrium nature, low gas temperature, the existence of reactive chemical species, and great selectivity, there is a significant potential to utilize these cold plasma sources in a broad range of applications (Kim and Ogata 2011).

2.4.4 Plasma components

These many species are made up of an electrified gas termed plasma, which consists of a chemically reactive medium, positive or negative ions, electrons, gas atoms, free radicals, and molecules in either their terrestrial or higher-order forms. It may be found in a huge variety of pressure and temperature conditions. So it can be generated at atmospheric pressure by the conjugation of energy with a gaseous media by using chemical, thermal,

nuclear, or radical means, or by electromagnetic waves injection or voltage application, to dissociate the gaseous media into electrons, ions, free radicals, photons, and atoms in the metastable state (Nehra *et al.* 2008). Figure 2.4 summarized the types of species in the plasma.

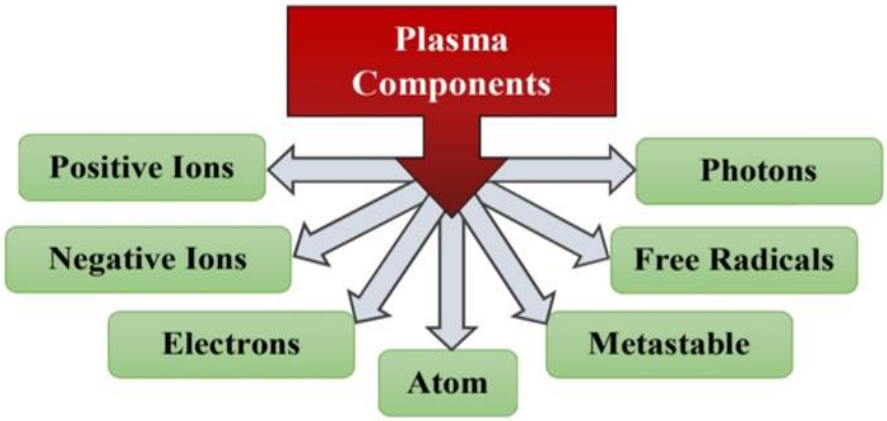

Figure 2.4 Plasma components

2.4.5 Method of production of atmospheric non-thermal plasma

2.4.5.1 Corona discharge

Corona discharge was the first scheme utilized to create ANTP. Depending on the polarity of the field and the electrodes' geometrical layout, it can take many different shapes. This kind of discharge is brought on by the electric field that surrounds inhomogeneous electrode configurations driven by a continuous or DC voltage, which is characteristic of an asymmetric electrode pair. An example is the point plane gap as shown in Figure 2.5, or the cylindrical wire gap. A low ionized plasma forms when the gas's breakdown strength is significantly exceeded by the strong electric field near the point electrode or wire electrode (Chang *et al.* 1991, Fridman *et al.* 2005).

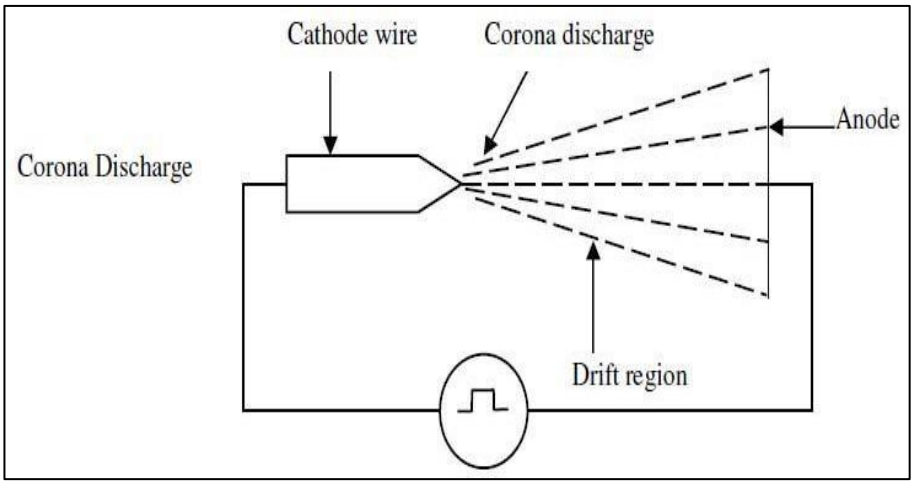

Figure 2.5 Schematic of corona discharge (Söderström 2008)

2.4.5.2 Dielectric barrier discharge (DBD) systems

A particular kind of AC discharge that produces non-equilibrium plasma at atmospheric pressure is the dielectric barrier discharge, also known as the barrier discharge. It has two electrodes in a set-up where at least one of them is situated in the current path between the metal electrodes and covered in a layer of dielectric (Figure 2.6) (Kogelschatz 2003). One of the key distinctions between a classical discharge and a DB discharge is that during a classical discharge, electrode etching, and corrosion take place because the electrodes are in direct contact with the discharge gas and plasma. In contrast, with DBDs the electrode and discharge are separated by a dielectric barrier, preventing corrosion and electrode etching. Another important difference is that the DBDs cannot operate with DC voltage because the capacitive coupling of the dielectric needs an alternating voltage to produce a displacement current (Söderström 2008).

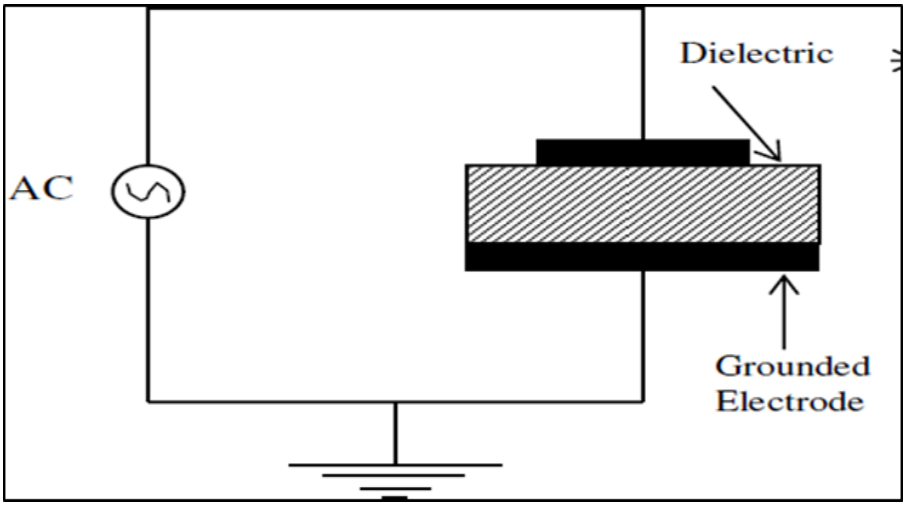

Figure 2.6 Typical electrodes arrangement of DBD configuration (Fridman *et al.* 2005)

2.4.5.3 Atmospheric pressure plasma jet (APPJ)

One of the three discharge types that may generate non-thermal plasmas is atmospheric-pressure plasma jets. In several ways, atmospheric pressure plasma is superior to low-pressure plasma. It may eliminate the costly Hoover operation and maintenance, enabling numerous creative designs to satisfy the expanding need for affordable, dependable, and simple-to-use plasma sources (Jiang *et al.* 2009). Also, it is not limited to chamber-based procedures. The ability of the plasma jets to produce non-thermal atmospheric pressure plasma, which can provide higher gas chemistry without needing to raise the gas temperature, is one enticing feature of the technology. Because of this beneficial property, low plasma temperature applications, such as those for material processing, biomedicine, or analytical reasons, have become quite popular. The plasma jet also provides the opportunity to launch reactive species outdoors, to a position that is unrestricted by anything, in contrast to certain other atmospheric plasma generators where the plasma is usually contained in the region between the electrodes or some sort of containment cage (Förster *et al.* 2005).

The schematic of the APPJ is shown in Figure 2.7. Between the two electrodes of the APPJ, gases such as helium, argon, oxygen, or other chemicals flow. In this configuration, the outside electrode is grounded, while the inner electrode is connected to the power source. A feedstock gas is moved between an outer grounded, cylindrical electrode and a

center electrode, producing a high-velocity effluent stream of highly reactive chemical species. This discharge results from the feedstock gas igniting (Brandenburg 2017).

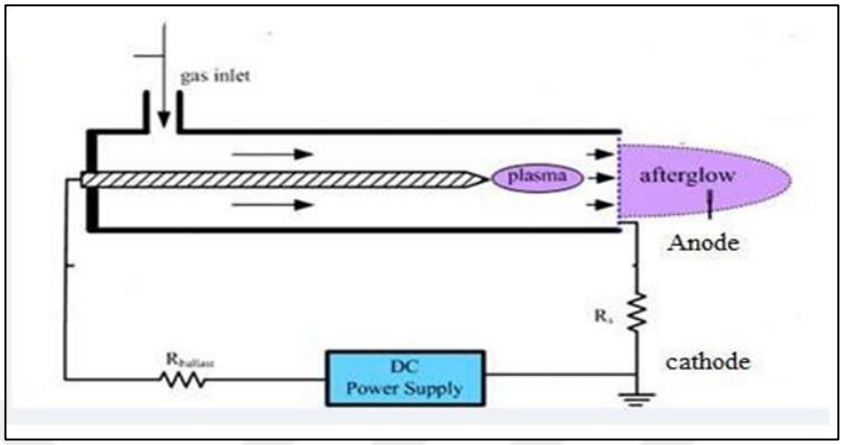

Figure 2.7 Schematic of atmospheric pressure plasma jet (Deng *et al.* 2013).

The main operating features of APPJ are as follows:

- Ionized gas from the plasma jet exits via the nozzle and is directed to the substrate for further processing.
- The electrode is not covered by a dielectric during operation, and there are no filaments, streamers, or arcs.
- The discharge gas's temperature ranges from 50°C, which allows it to treat delicate surfaces without causing harm, to 300°C, which enables it to treat sturdy materials considerably more forcefully (Schutze *et al.* 1998).

2.4.5.4 Plasma needle

A non-thermal atmospheric corona discharge, the plasma needle has a single electrode and may operate in a variety of gases. The fact that this type of plasma operates close to room temperature allows for the treatment of uneven surfaces and has a shallow penetration depth is one of its most crucial characteristics. Because of these advantages, the needle has a lot of potential for application in the biomedical field (Byrns *et al.* 2012). The plasma needle is made of sharpened stainless wire (1 mm in diameter). The powered

electrode, which is a wire, resides within a grounded metal cylinder that has an inner diameter of 1 cm and is positioned coaxially inside it. The cylinder is filled with flowing gas, as shown in Figure 2.8 (helium, argon, air, nitrogen, or hydrogen). At the metal needle's tip, plasma may be seen in the form of a 0.1 mm-diameter weak light. It can be used to etch materials, activate polymer surfaces, and treat live cells due to the aforementioned advantage (Shashurin *et al.* 2008).

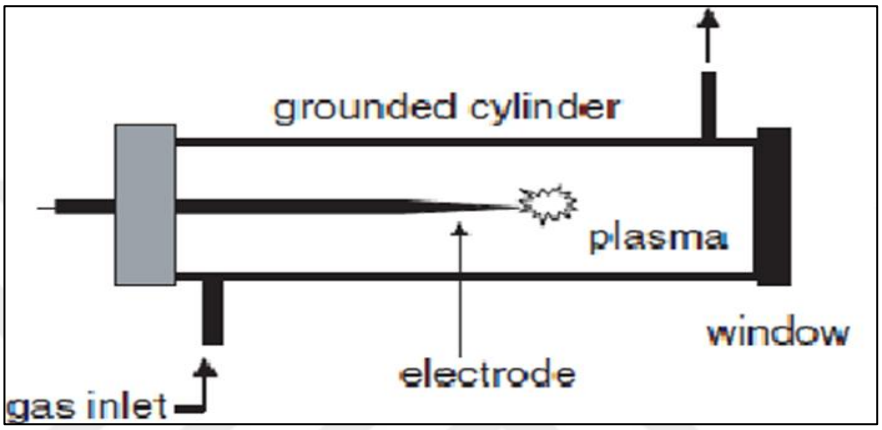

Figure 2.8 Schematic diagram of non-thermal plasma needle (García-Alcantara *et al.* 2013)

2.4.6 Characteristics of plasma

To confirm that the asset that contains charged particles represents the plasma, it should be subject to some conditions and rules:

2.4.6.1 Collective behavior

Plasma particles exhibit a simultaneous responses to the external stimulus, This indicates that there are several interactions between each plasma particle. In this way, it shows collective behavior. The microscopic result of an external stimulus can show the cooperative response of plasma particles. It can be referred to wave processes and plasma particles mutual shielding as examples of collective behavior (Takai *et al.* 2013).

2.4.6.2 Quasi-neutrality

Neutral gases are ionized to create plasma, which typically has an equal number of positive and negative charge carriers. The fluids with opposing charges are highly mixed in this condition and must resort to electrically neutralizing one another by the Debye length. This plasma is classified as "quasi-neutral," with the emphasis on "quasi" since some types of plasma modes are significantly affected dynamically by the slight deviation from precise neutrality (Callen 2006). In a system with dimensions (L) that are much larger than the Debye length, local concentrations of charge or external potentials are shielded out at a distance shorter than L. Much of the plasma is devoid of strong electric potentials or fields and is therefore largely neutral. The plasma outside of the sheath is "quasineutral," or neutral enough to allow for the existence of ni-ne-n, where n is a common density known as the plasma density (Tokunaga *et al.* 2022).

2.5 Atmospheric Micro Plasma Discharge

The method which is widely used for processing materials is atmospheric-pressure plasma, because of its low cost and easy usage. They have opened up new pathways for the synthesis of nanomaterials, because of recent progress in microscale plasma termed "Micro Plasmas"Micro plasma is a particular kind of plasma in which one of the dimensions is less than a millimeter. Microplasma exhibits some beneficial characteristics such as high electron densities in atmospheric pressure. The reactive radical species that can produce nanoparticles may be produced more easily when high-energy electrons (10 eV or more) are present (Alexandre *et al.* 2018). In this work, silver nanoparticles (Ag NPs) were produced between two electrodes using an atmospheric pressure non-thermal plasma glow discharge. Compared to other creation techniques, stable atmospheric micro plasma discharge production is a relatively safe, easy procedure (Alexandre *et al.* 2018).

2.6 Nanotechnology

The Greek term "nano" means "dwarf" in a very tiny sense, while the word nano denotes items from the billion (10^{-9} nm) in the average size. "Nanotechnology" is the creation and use of materials, machines, and devices on a nanometer scale, paying attention to the unique properties that occur to the structures in those small dimensions. The materials in the nanoscale have different (physical, chemical, and biological) properties that don't appear in their bulk state (Khanna 2016). Nanomaterials have wide applications in biomedical, catalysis, agriculture, electronic and optical fields. Traditional physical, chemical, and biological processes may be used to create nanoscale materials, biological and other hybrid processes, due to the development of novel methods and instruments for the synthesis, characterization, and manipulation of nanomaterials during the last two decades, and have expanded rapidly (Filipponi *et al.* 2010).

2.7 Nanostructures

A structure is considered to be nanoscale if at least one of its dimensions is between 1 and 100 nm. It is vital to distinguish between the various Nano-dimensions to characterize the architecture of nanoparticles.

According to the dimensionality, the following categories are known:

Quantization occurs in all three dimensions in a zero-dimensional object, often known as a quantum dot or "quantum box" (Wei *et al.* 2009).

Quantization occurs in two directions in a one-dimensional (1D) structure or quantum wire, resulting in just one direction of free motion.

A two-dimensional (2D) structure or quantum well, where the motion of the particle is quantized in one dimension but unconstrained in the other two.

A bulk structure or three-dimensional (3D) structure The particle is free since there was no quantization of the particle travel.

The type of nanostructure and density of states are shown in Figure 2.9 (Filipponi *et al.* 2010).

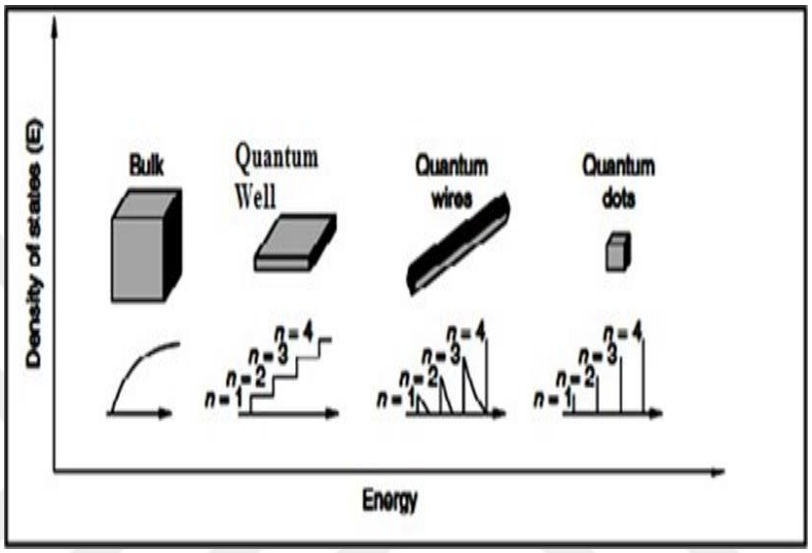

Figure 2.9 Electronic density states and quantum confined systems as a function of dimension (Filipponi *et al.* 2010)

2.8 Methods of Synthesis Nanoparticles

The synthesis of NPs opened alternative methods in the design of materials with new properties. Nanoparticles can be manufactured and each method differs from the other in terms of final product attributes and manufacture of various nanomaterials, thin films, and nanocomposites. Synthesis methods functions are very important in controlling the surface area and size of nanomaterials to use them in the desired applications including medicine, catalysis, and electronics. Nanoparticles and nanocrystals are prepared in many ways, physical, chemical, and biological (Khandel *et al.* 2018), as shown in Figure 2.10. Improving nanoparticle synthesis to have better control over particle size, distribution, shape, purity, quantity, and quality by adopting environmentally friendly, economically viable technologies has long been a challenge for researchers (Khan *et al.* 2019).

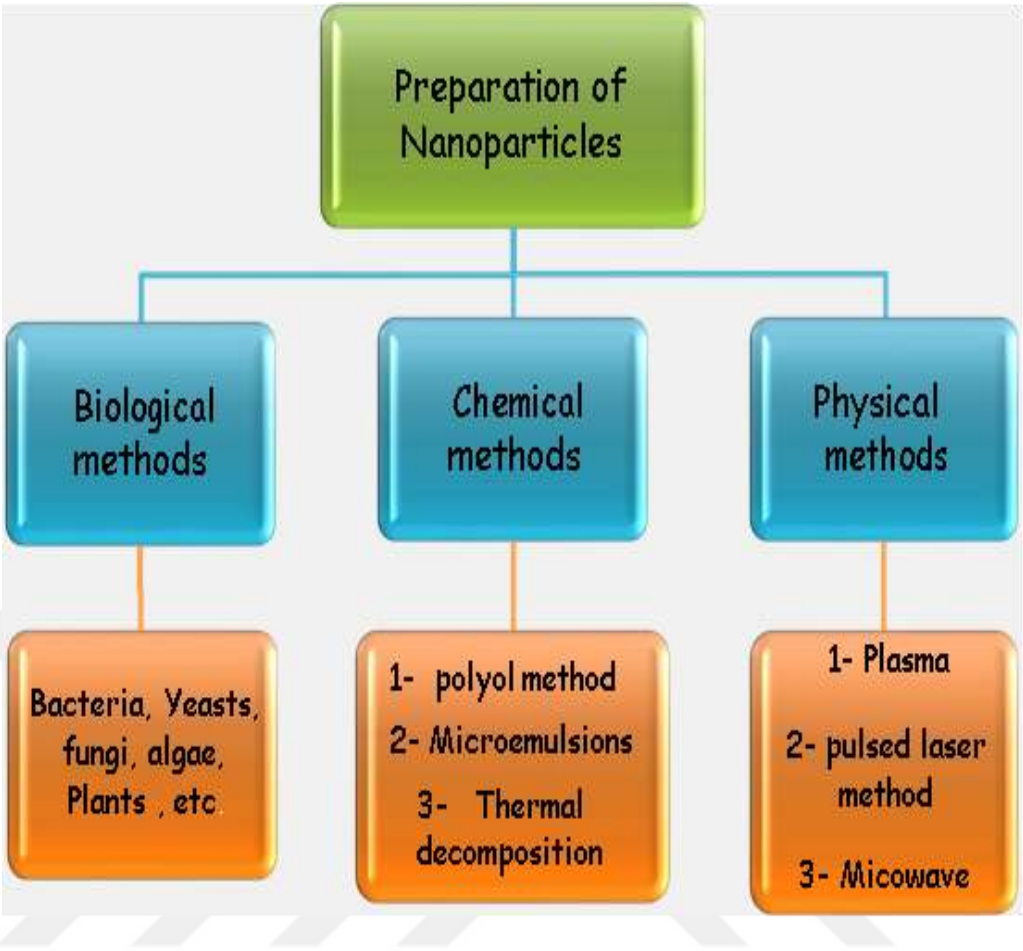

Figure 2.10 Different methods used in nanoparticles synthesis (Khan *et al.* 2019)

2.9 Approaches for Synthesis Nanoparticles

Two approaches are employed to create nanoparticles, as indicated in Figure 2.11 (Hornyak *et al.* 2018).

2.9.1 Top-down approaches

In this method, the bulk material is reformed to create nanomaterials after being partially disassembled, treated, produced, or deposited. This method involves applying an external force to a solid substance, which causes it to disintegrate into smaller particles. The defects in the surface structure and the fact that the nanoparticles are created from larger entities without atomic control are the technique's drawbacks and harm. Due to the extremely high surface-to-volume ratio of nanoparticles and nanostructures, these

imperfections will have a major impact on their surface chemical and physical properties. These flaws increase the difficulty of designing and producing devices (Ngô and Van de Voorde 2014).

2.9.2 Bottom-up approaches

This technique relies on atomic or molecular changes to create nanoparticles. Catalysts, electric/magnetic fields, and stress fields are a few common tactics. Top-down approaches are far more expensive, while bottom-up approaches must be able to build devices. Diverse synthesis and processing techniques often produce material that differs noticeably in terms of its chemical composition, microstructure, and crystallization. The substance demonstrates various physical characteristics as a result. In the production and handling of nanomaterials and nanostructures, the bottom-up approach is crucial (Guozhong 2004) (Figure 2.11).

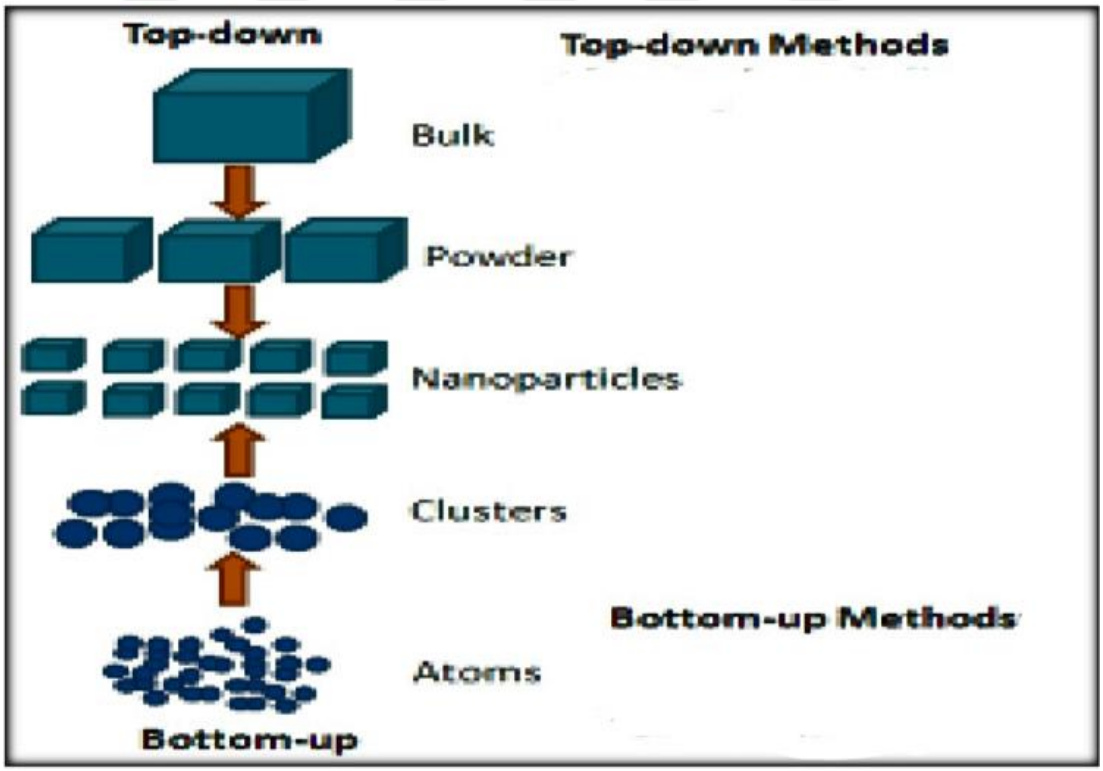

Figure 2.11 Schematic of the top-down and bottom-up approaches for the manufacturing of metal nanoparticles (Guozhong 2004)

2.10 Properties of Nanomaterials

Due to the quantitative influence of nanoparticles and an increase in the surface-to-volume ratio, the properties of mechanical, electrical, and magnetic nanomaterials as well as the melting point are drastically different from their equivalents of matter in natural size. Therefore, when the material is at the nanoscale, the previously mentioned properties are significantly improved, which has resulted in a rise in the demand for nanotechnology materials in industrial applications that depend on mechanical properties. Additionally, compared to the original material, nanomaterials have better optical characteristics (Gubicza 2017).

The size and form of nanoparticles have a significant impact on nanomaterials. It is very important to control not only the size of the particles but also the shape and nature of their surface, the purity of the solvent substance and its cleanliness in addition to the temperature of the solution, the concentration of the mineral salt, a factor. The size and shape of the nanoparticles also depend on the extent of interaction with the stabilizers and the surrounding medium, as well as the style and method of preparation. Reduction and reaction time all have an impact on particle size, and it is still difficult to manage the size and form of nanoparticles (Senapati *et al.* 2004).

The materials' novel features and properties, including color change, electrical and magnetic properties, thermal conductivity, insulation, melting point, light reflection, degree of hardness, strength, transparency, etc., are acquired at the nanoscale level. These materials also have considerable advantages in terms of applications (Wei *et al.* 2009).

Comparing nanoparticles to the same volume of the substance, they have a disproportionately high surface area. For illustration, consider a sphere with a radius of:

- The surface area of the sphere becomes $4\pi r^2$
- The volume of the sphere equal to 4/3 (πr^3)
- Subsequently the surface area to the volume ratio=$4\pi r^2/(4/3\ (\pi r^3))=3/r$

This implies that by lowering the radius of the sphere, the surface area to volume ratio rises. Here, it can also be deduced that surface area grows when it is believed that volume is divided into smaller portions. Then, when particle size reduces, more atoms are discovered at the surface than inside as opposed to within as particle size decreases (Koole *et al.* 2014).

The maximum surface area of nanoscale particles maximizes their potential for reaction. Creating novel materials and streamlining chemical processes are both made possible by the large surface area-to-volume ratio of nanoparticles. More atoms in ordinary materials are created at depth rather than at a surface. Its bulk disappears in nanomaterials. Indeed, a single layer of atoms on surfaces is often the focus of nanotechnology. Materials having this feature are special. For instance, they could serve as highly efficient catalysts, be used to create thin films that serve as heat barriers or boost resistance to prevent materials from deteriorating (Ridley *et al.* 2006).

2.11 Antibacterial Activity of Silver Nano Particles

Infectious illnesses have spread widely as a result of the rise in multi-antibiotic resistance bacteria, posing a serious threat to global human health. The creation of novel antibiotics should continue since they are crucial to preserving the efficiency of antimicrobial therapy. Yet, historical experience has demonstrated that new antibiotics may only be effective for a short time. Hence, the need for novel strategies to stop microbial proliferation became critical (Ryskova *et al.* 2010).

Effects of silver nanoparticles on microorganisms by the specific method by which silver nanoparticles exert their antibacterial properties is unclear. However, there are several theories regarding how silver nanoparticles work with bacteria to produce a microbicidal effect. Silver nanoparticles may adhere to the bacterial cell wall and then penetrate it to produce structural changes in the cell membrane, such as increased membrane permeability and cell death. This could result in "pits" and an accumulation of nanoparticles on the cell's surface (Prabhu and Poulose 2012). Another way that cells could die is if the silver nanoparticles produce free radicals. Free radicals are created

when silver nanoparticles interact with bacteria, according to a study employing electron spin resonance spectroscopy. Cell death might result from these free radicals' capacity to damage cell membranes and render them permeable. Moreover, it has been proposed that the nanoparticles may release silver ions that may then interact with the thiol groups of several important enzymes to make them inactive (Feng *et al.* 2000). When bacteria come into touch with silver, the silver ions they absorb disrupt various cellular processes and cause cell damage. A respiratory enzyme may be inhibited by silver ions, which results in the production of reactive oxygen species, which assault the cell directly. As silver is a soft acid, it will inevitably react with a soft base because an acid's inherent propensity is to do so (Morones *et al.* 2005). Sulfur and phosphorus, two soft bases, make up the majority of the components of the cells. The response that results in cell death may be brought on by the effect of these nanoparticles on the cell. Moreover, since phosphorus and sulfur make up a large portion of DNA, nanoparticles may act on these soft bases to damage DNA, which would invariably result in cell death (Prabhu and Poulose 2012). Bacterial DNA replication problems can be caused by interactions between silver nanoparticles and the phosphorus and sulfur in DNA, which may lead to the eradication of the germs. Also, it has been found that nanoparticles can change how bacteria transmit signals. It is generally known that bacterial signaling is impacted by the phosphorylation of protein substrates. Dephosphorylation only occurs in the tyrosine residues of Gram-negative bacteria. The nanoparticles change the phosphotyrosine profile of bacterial peptides. It has been shown that the tyrosine residues in the peptide substrates are dephosphorylated by the nanoparticles., which prevents signal transduction and halts proliferation. Nonetheless, it is crucial to understand that further research is required to completely understand the problem (Shrivastava *et al.* 2007) (Figure 2.12).

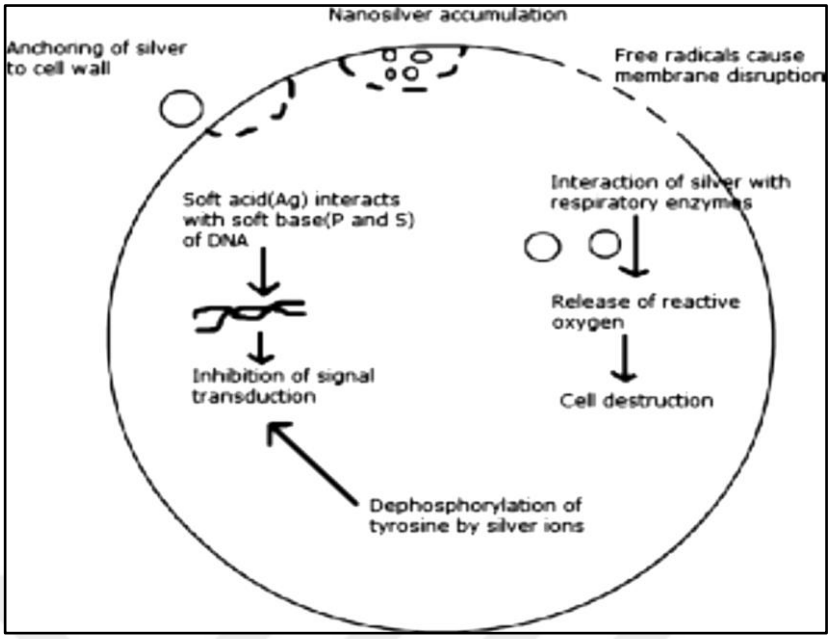

Figure 2.12 Several ways that silver nanoparticles affect microorganisms (Prabhu and Poulose 2012).

2.12 The Bacteria

Clinically isolated bacteria *Staphylococcus aureus* and *Escherichia coli* were used in the experiment.

2.12.1 *Escherichia coli*

Escherichia coli is the most prevalent member of the Enterobacteriaceae family to be found in the normal gut flora as well as the most common source of opportunistic infections. All members of the Enterobacteriaceae family are facultative, all of them ferment glucose, all of them turn nitrates into nitrites, and all of them lack oxidase (Sherris 1984).

Sporing but negative for gram most strains of the bacillus *Escherichia coli* are motile and generally have both sex pili and sticky fimbriae (Mahon and Manuselis 1995). The majority of strains rapidly ferment lactose, resulting in colonies that are smooth, glossy, transparent, and rose-pink when cultivated on MacConkey medium. Certain strains that

are cultivated on blood agar cause hamolysis zones that encircle the colonies. Colonies on cystine-lactose-electrolyte deficient (CLED) media are smooth, spherical, and 1-1.5 mm in diameter, and if lactose is fermenting, they are yellow opaque (blue, if non-lactose fermenting) (Mackie and McCartney 1989).

The majority of the aerobic commensal bacteria in a healthy gut are *Escherichia coli* strains (Mackie and McCartney 1989).

Escherichia coli, formerly believed to be a benign part of the colon flora, is now connected to a broad variety of illnesses and infections, including bacteremia infections in individuals of all ages, meningeal, gastrointestinal, urinary tract, wound, and urinary tract infections (Mahon and Manuselis 1995).

Peritonitis, cholecystitis, septic wounds, and bedsores are some of the other illnesses brought on by *Escherichia coli*. They may also result in bacteremia, endotoxic shock, or an infection of the lower respiratory tract, especially in surgical or weakened patients (Mackie and McCartney 1989) (Figure 2.13) (Table 2.2).

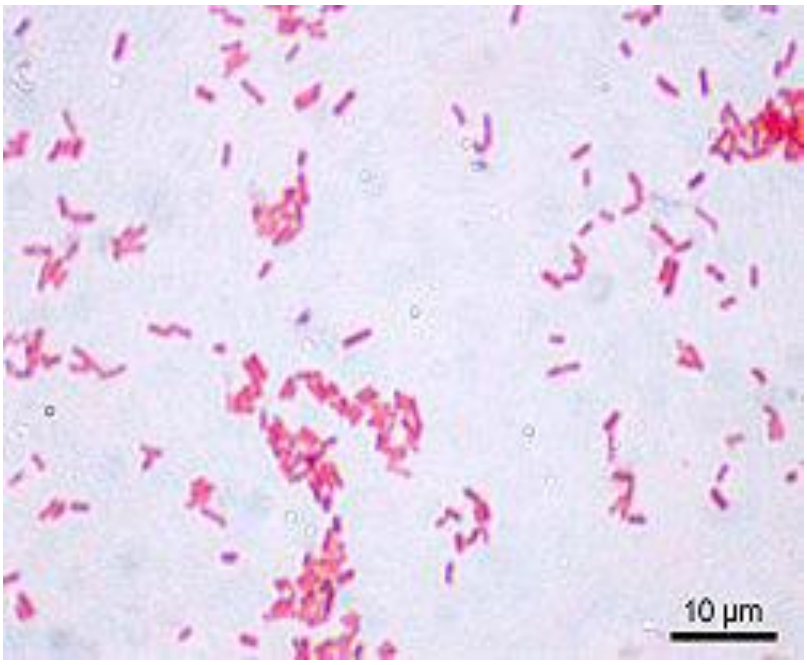

Figure 2.13 Gram stain of *E. coli*

Table 2.2 Classification of *E. coli*

Domain	Bacteria
Phylum	Proteobacteria
Class	Gramma proteobacteria
Order	Enterobacteriales
Family	Enterobacteriaceae
Genus	Escherichia
Species	coli

2.12.2 *Staphylococcus aureus*

Gram-positive cocci belonging to the genus Staphylococcus (staphylococci) often cluster together in grape-like formations (Ryan and Ray 2004).

Staphylococci are rounded cells with a diameter of about 1 μm, arranged in random clusters. Moreover, single cocci, pairs, tetrads, and chains of cocci may also be seen in liquid cultures. Cocci stain heavily gram-positive while they are young; as they become older, many of their cells change to gram-negative. The bacteria Staphylococci do not produce spores and are not mobile (Brooks *et al.* 2007).

As a facultative anaerobe, *Staphylococcus aureus* prefers a pH of 7 and a temperature of 37°C for growth. The origin of the species name Aureus is the white colonies that *S. aureus* creates, which have a propensity to become a buff-golden hue over time. Most strains, but not all, exhibit a visible ring of hemolysis around the colony (Ryan and Ray 2004).

Colonies are 1 to 3 mm in diameter on nutritional agar after aerobic incubation for 24 hours at 37°C. They have an entire edge, a smooth glistening surface, and an opaque pigmented look. The majority of types have golden coloring with orange, yellow, and cream variants. Colonies are tiny to medium in size and pink to pink-orange on MacConkey agar (Mackie and McCartney 1989).

Extremely effective colonizers of both people and animals. Their primary habitat is the skin, especially moist places like the axilla, groin, and anterior nares (nose). These organisms are carried by between one-third and three-quarters of people at any given moment. Staphylococcal infections happen everywhere, and newly discovered multiresistant or hypervirulent strains disperse quickly over large geographic areas. Since the bacteria may survive for days in the air, on objects, or in dust, they can contaminate areas (like hospitals) and spread over long periods. Certain individuals may shed the organism more frequently than others. The origins of staphylococcal infections are either internal (endogenous) or external (exogenous) (Irving *et al.* 2004).

S. aureus causes severe infections of the skin, soft tissues, bones, lungs, heart, and brain (Irving *et al.* 2004). include septic arthritis, which is frequent in children and those with a history of rheumatoid arthritis, endocarditis caused by bacteremia and subsequent pneumonia, osteomyelitis brought on by bacteremia, and pneumonia. Both the syndrome of toxic shock and the syndrome of scalded skin are conditions brought on by staphylococcal toxins (Sherris 1984) (Figure 2.14) (Table 2.3).

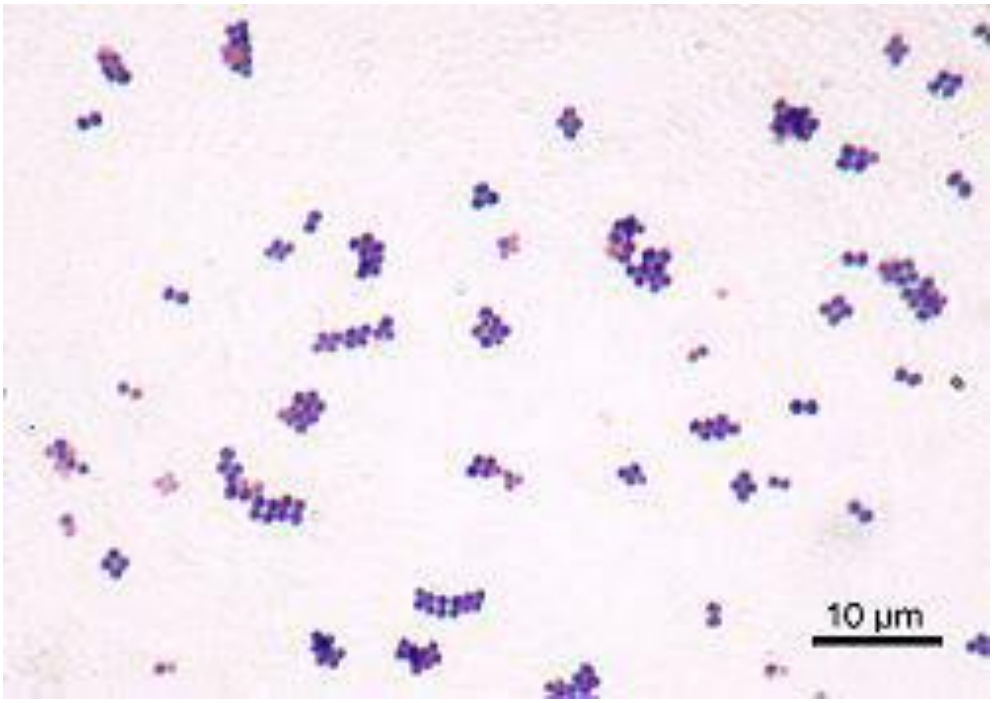

Figure 2.14 Gram stain of *S. aureus* cells

Table 2.3 Classification of *S. aureus*

Domain	Bacteria
Phylum	Firmcutes
Class	Bacilli
Order	Bacillus's
Family	Staphylococcaceae
Genus	Staphylococcus
Species	aureus

2.13 The Measurement Techniques

Nanoparticles' physicochemical properties are crucial for their behavior, biodistribution, safety, and effectiveness. The features of Ag NPs are crucial since they assess the functionality of created particles. Several characterization methods, such as Energy Dispersive X-ray (EDX) Microanalysis, Field-Emission Scanning Electron Microscopy (FESEM) Analysis, and X-ray Diffractometric (XRD), must be used to examine the generated samples' varied characteristics. The ideas and use of several types of analytical methods for the characterization of Ag NPs have been described in several reputable publications and reviews.

2.13.1 X-ray diffraction (XRD)

One of the first techniques for examining the structure of solids is X-ray diffraction. Electromagnetic waves of a specific frequency are refracted. nonetheless, interact to create both positive interference (bright spots on the film) and negative interference (dark spots). It is possible to determine the values of network parameters (unit cell dimensions) by carefully analyzing the diffraction patterns. Figure 2.15 depicts a schematic of the crystal-level Bragg's law and X-ray diffraction. The electromagnetic waves known as X-rays, which occur between gamma and ultraviolet rays, have a definite wavelength in the range of 0.1 to 100 and comparatively high energy (Lehn 1993).

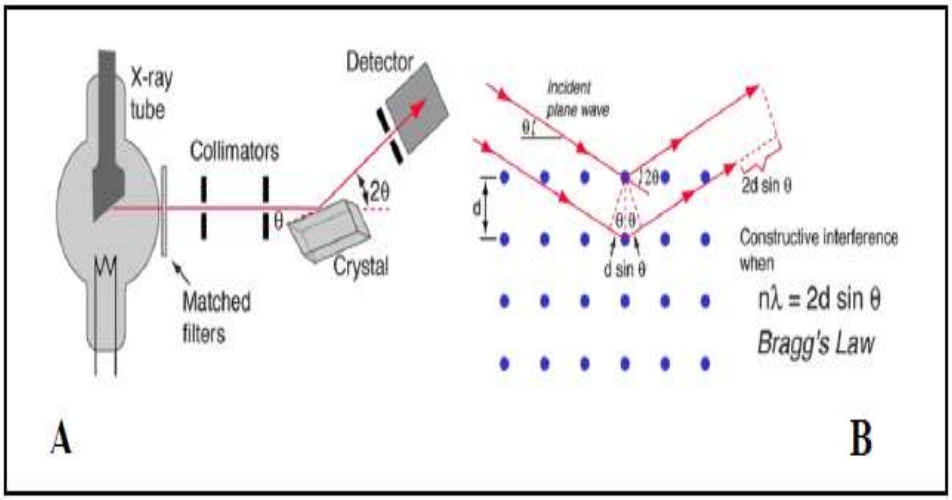

Figure 2.15 (A) X-ray diffraction diagram, (B) crystal levels and Bragg's law (Lehn 1993).

XRD is a vigorous technique utilized because of finding out the crystal structure of crystalline material using a diffraction test sample or for measuring. The structural characteristics of these phases, such as strain state, grain size, and distinct orientation, are non-damaging and don't need any elaborate setup. The particle size has an impact on the diffraction line's width, which increases as the particle size decreases owing to a loss of long-range arrangement relative to the crystal. XRD is used in the Deby Sherrer formulation to determine particle size as in Equation (2.1) (Zhang 2009):

$$D = \frac{0.9\lambda}{\beta \cos\theta} \qquad (2.1)$$

where is the Bragg angle, is the full-width half maximum (FWHM) of the peak in radians, D is the nanocrystal diameter and is the wavelength of light.

2.13.2 UV-VIS spectrometer

The absorption spectrum is measured by using a UV-VIS spectrometer. This spectrometer covers a wide range of the electromagnetic spectrum, from UV to NIR. The device contains two excitation sources:

(a) Deuterium lamp: that covers the range of wavelengths (190-360) nm

(b) Tungsten lamp: that covers the range of wavelengths (360-1100) nm

It is possible to use both lamps to cover the ranges (UV-VIS) spectrum. The device contains a monochromator to select the wavelength that excite the sample, also it contains a grating, filters according to the desired wavelength and a detector from a type of (PMT), and a power supply. The idea of measurement depends based on the separation of the incident beam into two beams, one of them passes through the sample and the other to the solvent that represents the reference. Finally, the device records the absorption spectrum to the samples (Ungula 2015).

2.13.3 Field emission-scanning electron microscope (FE-SEM)

A scanning electron microscope (SEM) is a device that is used to examine the morphology of a material at greater magnification, better resolution, and deeper focus than an optical microscope. Here, a small area of the sample's surface is scanned by a focused beam of accelerated mono-energetic electrons. The samples were dropped onto a silicon wafer and examined by field emission scanning electron microscopy (FE-SEM) at the Sharif University of Technology using a TESCAN BRNO-Mira3 LMU scanning electron microscope to determine the size of the particles or grains, the types of nanoparticles, and the surface morphology.

2.13.4 Dynamic light scattering (DLS)

The particle size in the submicron range is calculated using dynamic light scattering (DLS) and variations in the intensity of the scattered photons. The temperature and viscosity of the medium in which particles are disseminated play major roles in translational diffusion. The Einstein-Stokes equation may be used to determine the particle size since the root demonstrates that the square displacement of the particle is linked to the diffusion constant. The intensity-intensity correlation function, which may

be used to estimate the diffusion coefficient and, therefore, the particle size in the system, is determined by the variations in the intensity of scattered light. Modern DLS devices have been developed as a result of the use of numerous experimental and theoretical methodologies to measure the diffusion coefficient of particles in a solution (Karmakar 2019).

The particle size in the submicron range is calculated using dynamic light scattering (DLS) and variations in the intensity of the scattered photons. The temperature and viscosity of the medium in which particles are disseminated play major roles in translational diffusion. The Einstein-Stokes equation may be used to determine the particle size since the root demonstrates that the square displacement of the particle is linked to the diffusion constant. Modern DLS devices have been developed as a result of the many experimental and theoretical methods that have been used to measure the diffusion coefficient of particles in a solution over time (Harding and Jumel 1998).

2.13.5 Zeta potential

The liquid layer that surrounds the particle is made up of an exterior area (diffuse) and an interior region (Stern layer), where the ions are less tightly linked. A fictitious border separates the ions and particles of the diffuse layer into a stable unit. Ions within the border move the particle as it travels (for instance, because of gravity). The ions remain with the bulk dispersant outside of the barrier. This boundary has zeta potential (surface of hydrodynamic shear) (Figure 2.16).

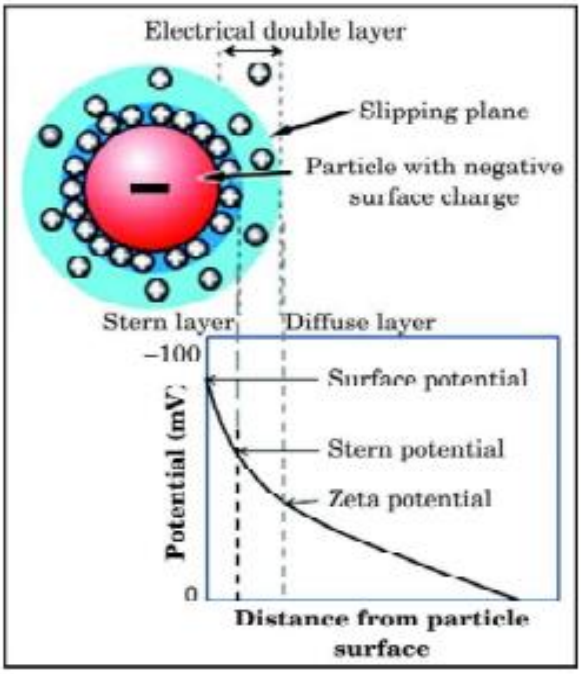

Figure 2.16 Schematic representation of the origin of zeta potential

The colloidal system's potential stability is indicated by the magnitude of the zeta potential. The propensity for the particles to attract one another and come together will be absent if all the particles in suspension have a large negative or positive zeta potential. Low zeta potential levels, on the other hand, will exert the least amount of force possible to keep the particles from aggregating and flocculating. The line separating stable and unstable suspensions is frequently drawn at +30 or -30 mV. Zeta potentials greater than or equal to +30 mV or greater than -30 mV are most frequently associated with stable particles. Particles having densities greater than the dispersion will eventually settle and form a densely packed bed (i.e., a hard cake), even if they are scattered. If the zeta potential of different materials is to be compared, the zeta potential of each particle must specify the nature of the dispersion as the zeta potential depends on both the surface and the dispersant (Karmakar 2019, Kaszuba *et al.* 2010).

2.13.6 Inductively coupled plasma mass spectroscopy

ICP-MS, also known as inductively coupled plasma mass spectrometry, is a method for analyzing elements in liquid or solution samples on both a qualitative and quantitative

level. ICP-MS was created in the late 1980s to combine the quick and simple analytical capabilities of ICP (Inductively Coupled Plasma) technology with the precision and low detection limits of a mass spectrometer (mass spectrometer) (Wilschefski and Baxter 2019). ICP often uses argon or other noble gases as the plasma gas because they effectively vaporize, dissociate, atomize, excite, and ultimately ionize the sample components for study. Furthermore, the high-temperature procedure applied, which may reach 7000 K, causes total fragmentation of every molecule in the sample, remaining only identifiable atomic components, such as metals, metalloids, or heteroatoms. The high-temperature ICP source and a mass spectrometer are combined in an ICP-MS. Multi-element analysis can be performed with the ICP-MS equipment up to part per trillion levels. Generally, argon gas has been heated to generate a plasma flame, which then converted the atoms of the elements to ions in the measured sample. After that, the ions are separated and identified by the mass spectrometer. Calibration with multi-element reference standards can be used to estimate the ion concentration of the samples.

ICP-MS is an attractive option for quantitative analytical detectors because it has a wide linear dynamic detection range, high sensitivity, and accurate detection and quantification of metals, metalloids, and heteroelements like non-metals, semi-metals, and halogens (Pröfrock and Prange 2012). Figure 2.17 shows a simple schematic of the instrument.

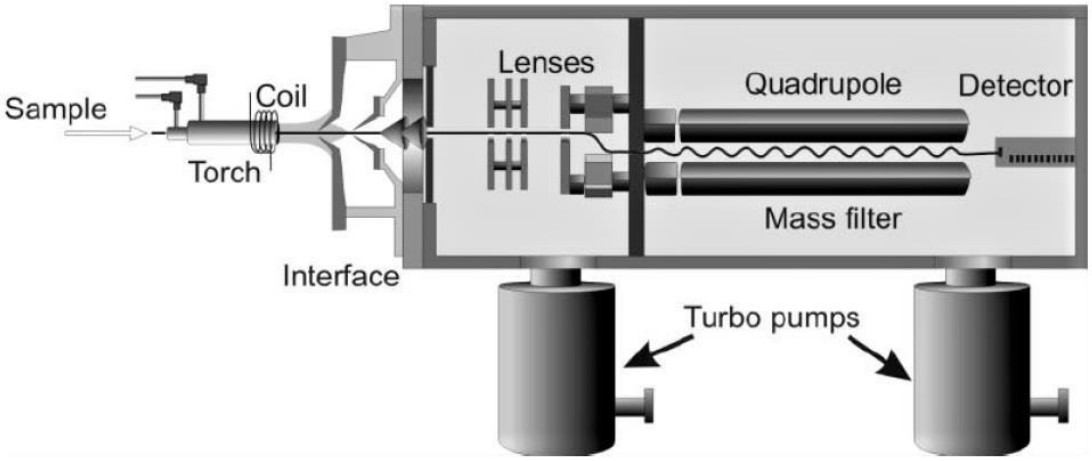

Figure 2.17 Schematic diagram of an ICP-MS technique cross-section

2.14 Medical Application of Nanoparticles

Nanoscience has led to a technological revolution in the world, dealing with materials with highly improved physical, chemical, and biological properties. Many basic applications are used with nanoparticles in the application of biochemistry, for example, medication and tumor treatment (Tang and Feng 2014).

Nanoparticles can target and penetrate certain organs and cells, which can be exploited in nanomedicine Nanoparticles are currently used in medical sciences in a variety of ways, including imaging, sensing, gene delivery systems, targeted drug delivery, and artificial implants. Nanoparticles can be formed of metals, polymers, or ceramics. The transport of drugs and genes, the treatment of cancer with gold nanoparticles, fluorescent biological labels, and the bio-detection of pathogens, food components, and cosmetics are just a few examples of nanoparticles utilized in the pharmaceutical industry (Nejati *et al.* 2022).

3. MATERIALS AND METHODS

This chapter describes the materials and procedure utilized to produce Ag NPs using an atmospheric pressure plasma jet, as well as the instruments and measurement techniques that were used to evaluate the structural, morphological, and optical features. Using synthetic silver nanoparticles on bacteria for biological purposes is another option. A schematic of the experimental study is shown in Figure 3.1.

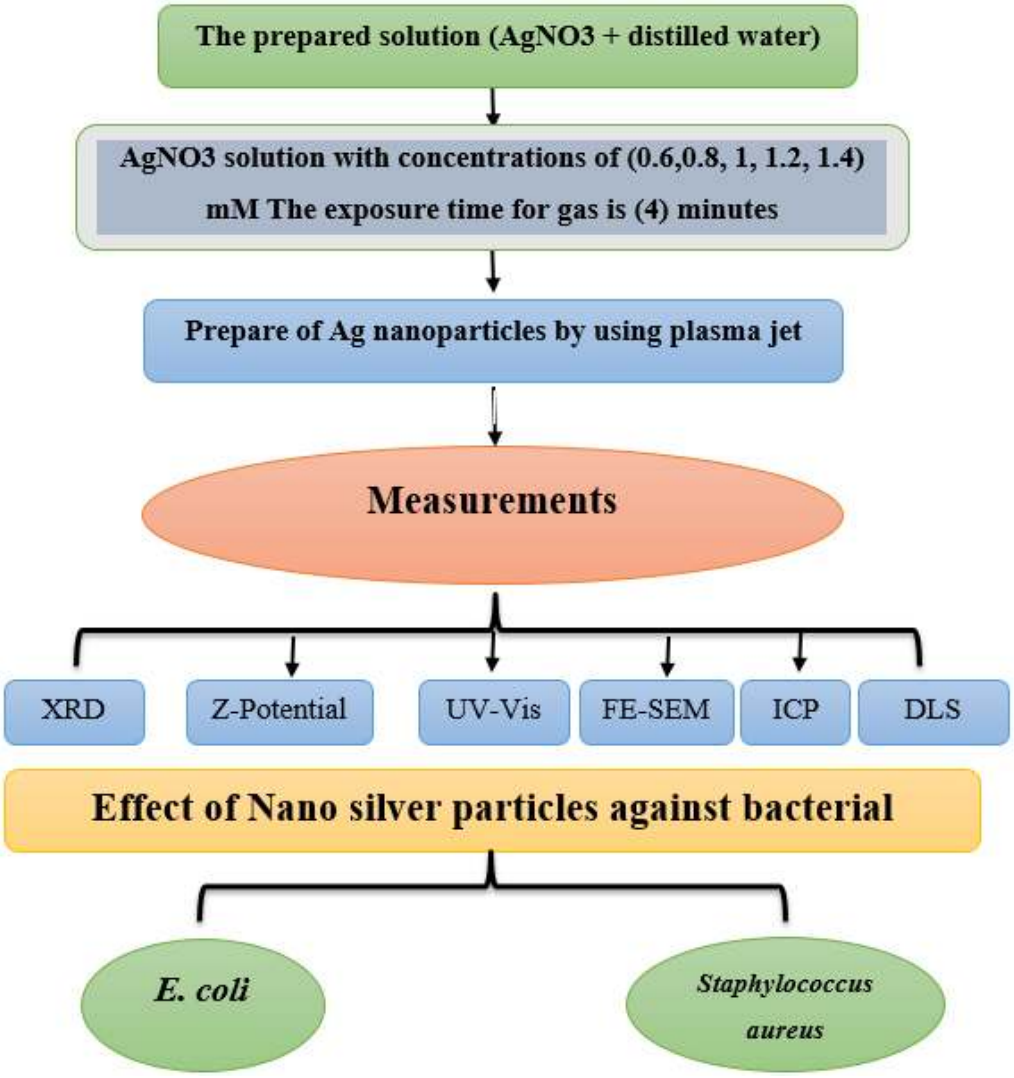

Figure 3.1 Diagram of the experimental work and procedures

3.1 Plasma Jet at Atmospheric Pressure in Liquid Technique

Aqueous solutions of $AgNO_3$ were prepared in different concentrations (0.6, 0.8, 1, 1.2, 1.4 mM) respectively, and time 4 min of plasma exposure. The plasma system diagram used for the synthesis of Ag nanoparticles is shown in Figure 3.2.

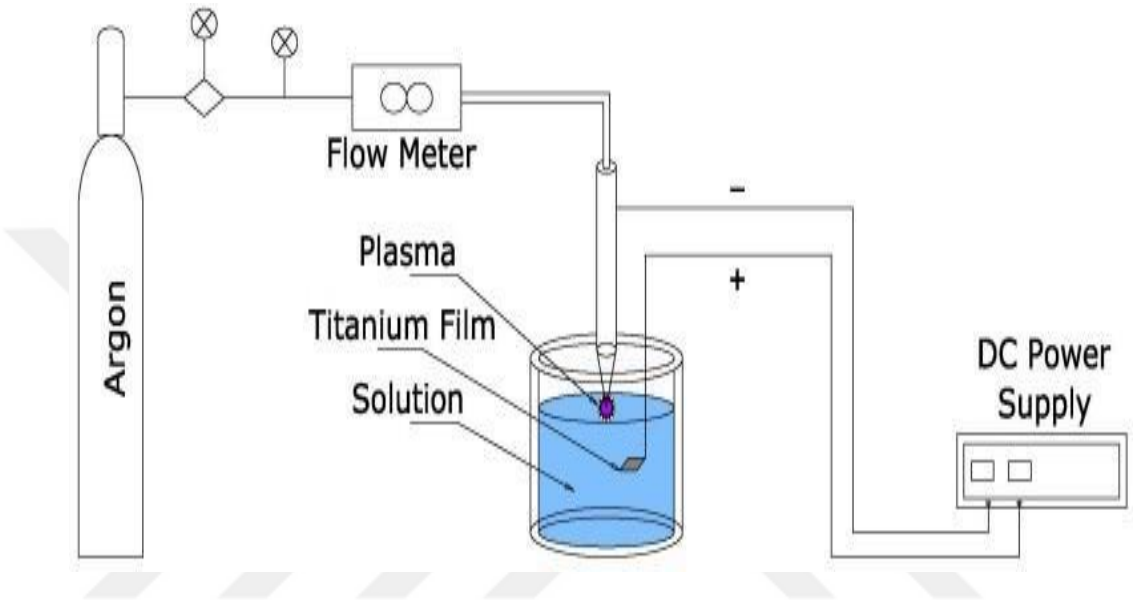

Figure 3.2 Operation of plasma system under atmospheric pressure

The working system of non-thermal plasma includes the following parts:

- Argon gas contained a gas outlet containing a regulator to control the speed of exit gas.
- Flow meter which controls the gas flow with a calibrator of (1-5 Litter per minute) which connects to the hollow tube. We used a calibrator of (1.5 min/L), the end of the hollow tube which connects to a stainless steel tube.
- The distance between the tip of the stainless steel tube and the surface of the solution was maintained at 1 cm. The stainless steel tube had an inner diameter of 1 mm, and a length of 3 cm, and was linked to the negative terminal of the power supply.
- A square piece of stainless steel foil (its dimension 1cm x1 cm) was immersed attached to the positive terminal of the power source and dissolved in the prepared solution.

- Glass beaker, The beaker was placed upon the movement stage under the stainless steel tube, and the stainless foil is placed in the beaker filled with 10 mL of the prepared solution. The depth of the stainless steel foil under the solution is about 2 cm.
- DC Power supply with a high voltage of about 6 kV.

The picture of the experimental setup is shown in Figure 3.3. The plasma was generated at the surface of the prepared solution and the end of a stainless steel tube. While the electrons move to the anode when the plasma was formed, the ions on the liquid's surface work to reduce the nanomaterial.

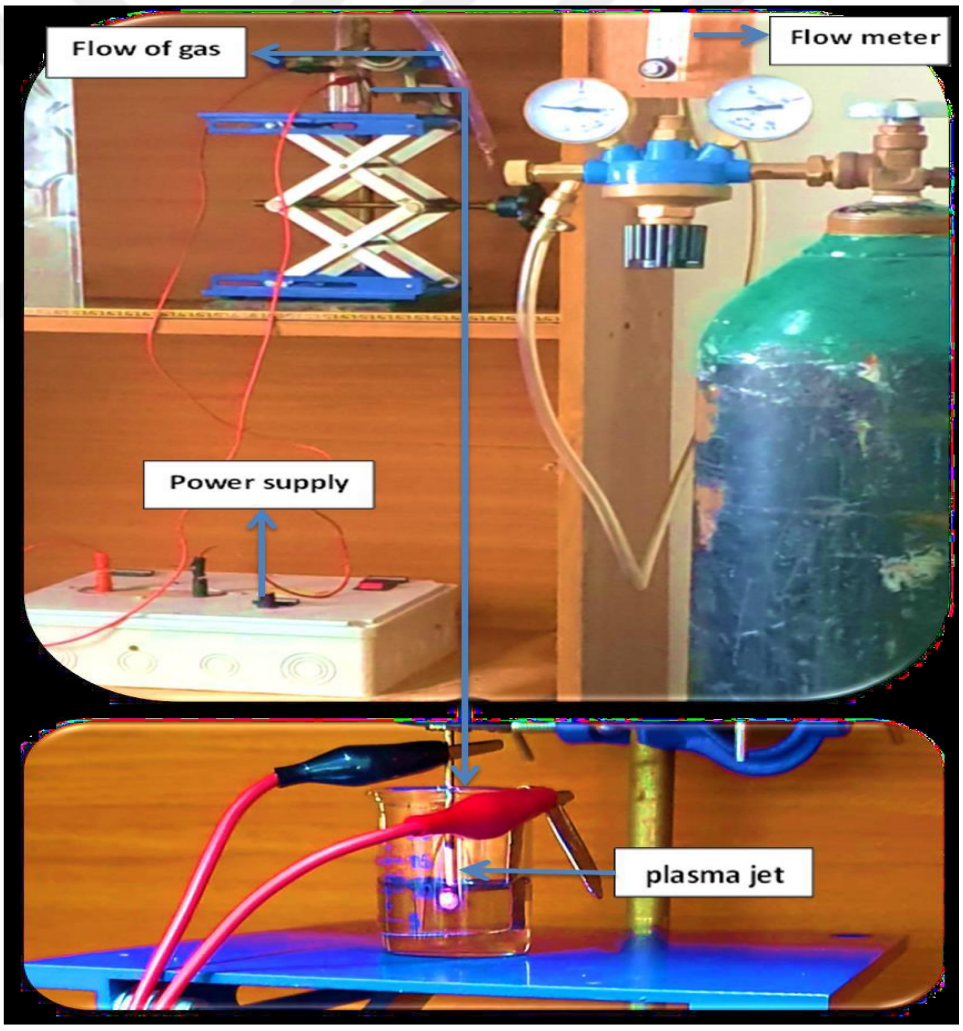

Figure 3.3 Experimental set-up of a plasma jet in liquid

3.2 Materials

99% pure silver nitrate ($AgNO_3$) produced by a German manufacturer was utilized (molecular weight: 169.88 gm/mol, color: White, Easily soluble in cold water). $AgNO_3$ was used as a metallic precursor for the preparation of Ag NPs.

3.3 Preparation $AgNO_3$ Aqueous Solution

Aqueous solutions of $AgNO_3$ were prepared in different concentrations (0.6, 0.8, 1,1.2, 1.4 mM) respectively with a volume of 100 mL of deionized water, and Equation (3.1) was used to calculate the required weight with a molecular weight of 169.88 gm/mol.

$$m = \frac{C \times V \times M_w}{1000} \tag{3.1}$$

Where:

- m: The amount of the dye needs to obtain the desired concentration in (g).
- V: The volume of solvent needed to add to the dye in (liter).
- M_w: Molecular weight of the dye used in (g/mol).
- C: the dye concentration (mole/liter).

Also, fructose was added to the solution as a stabilizing agent prepared with 0.018 gm and mixed with $AgNO_3$ solution to prevent Ag nanoparticles from aggregation, and then the solution was moved by stirrer carefully to get homogeneity of solution.

3.4 Synthesis Ag Nanoparticles Colloidal

The synthesized silver nanoparticles (Ag NPs) by CAP, requires applying a high voltage of about 6 kV, when the circuit of Cold plasma was switched on, plasma was formed between the stainless steel tube and the aqueous solution of $AgNO_3$. The high-energy

electrons and charged ionic (Ar) in the plasma help in completing the circuit and a current starts flowing in the system. After a few minutes of plasma exposure to the aqueous solution $AgNO_3$, the color of the solution is changed to dark brown which is the property of Ag NPs formation shown in UV–Vis absorbance. The color change is shown in Figure 3.4. To study the effect of the concentration and the time exposure of the plasma on the characteristic of Ag NPs, five different concentrations (0.6, 0.8, 1,1.2, 1.4 mM) with time 4 min. The obtained silver nanoparticles colloidal were then taken for examination and investigation.

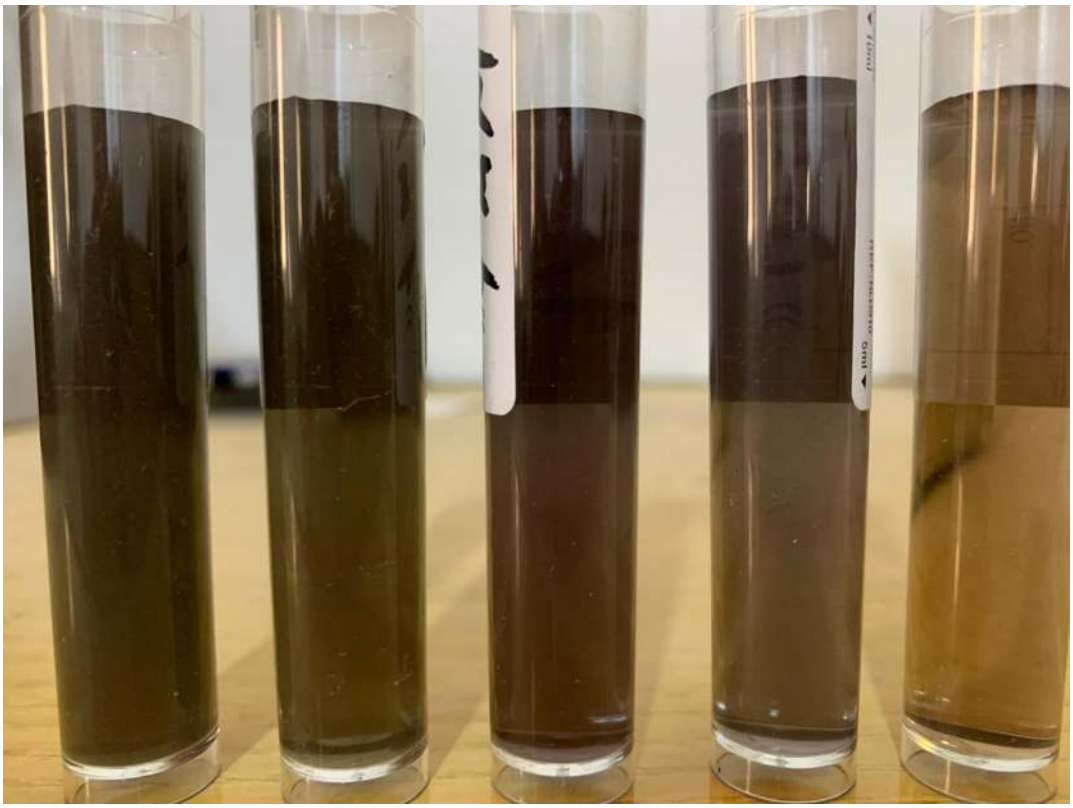

Figure 3.4 The solution colors of the samples plasma exposure (4 min) with different concentrations (0.6, 0.8, 1,1.2, 1.4 mM)

3.5 Preparation of the Substrate

3.5.1 Preparation of silicon substrate

The solution containing the silver nanoparticles was placed on a silicon wafer for use in XRD and FESEM measurements to analyze the structural and morphological characteristics of the produced silver nanoparticles. The steps below were used to meticulously clean N-type silicon wafers:

- The silicon substrates were cut into squares with a size of 2x2 cm^2 approximately.
- Silicone substrates were immersed in distilled water and placed in an ultrasonic machine for 15 minutes.
- The silicon substrates were cleaned by immersion in the acetone bath for 10 minutes, to remove any remaining impurities on their surface.
- The silicon substrates were cleaned by immersion in an alcohol high-purity bath and placed in an ultrasonic machine for 15 minutes, remove the substrates from the alcohol and rinse in distilled water to make sure that the impurities and residuals are removed from their surface.
- The silicon substrates were dried carefully and wiped by optical soft tissue.

3.5.2 Spin coating

Using the Drop Casting process, a thin layer of the silver nanoparticle-containing solution was applied to silicon substrates. The solution was first placed in the ultrasound machine to achieve homogeneity of the solution, then the solution was withdrawn by the dropper to be precipitate on a silicon wafer. It was heated to a temperature of 39°C to dry completely. After it dries, another drop of silver nanoparticles solution was placed and left to dry, and the process was repeated to obtain thin layers of the prepared solution.

3.6 Bacteria Isolates

These types of bacteria can induce infections and provide a gratifying experience. These bacteria were acquired from the Ministry of Health in Anbar, Iraq's AL-Fallujah Teaching Hospital. Both the *Staphylococcus aureus* and the *Escherichia coli* bacterial suspensions that were used in the synthesis used concentrations that were specified. To examine the effects of silver nanoparticles on bacterial samples, 50 mL of the nanoparticles were put into a well in a petri dish containing bacteria disseminated on agar using a cotton swab. Using a digital caliper Z11155 (Lidl, UK), the approximate diameter of inhibition zones (zones free of bacterial growth) was calculated. Advanced imaging software (Image-J program) was used to compute the diameter of inhibitory zones to improve measurement accuracy for irregular zones. Depending on what this test mentions, 0.1 mL of bacterial suspension from both *Escherichia coli* and *Staphylococcus aureus* should be spread on solidified Mueller-Hinton Agar and left to dry for 5 minutes. The 6 mm holes in the seeded agar were made with a steel tube. After planting the medium, various quantities of silver nanoparticles were added to each well, and the plates were left at room temperature for 1 hour to allow for diffusion before being placed in the incubator at 37 degrees Celsius for 24 hours. The resulting inhibitory zones were calculated in millimeters (mm).

3.7 Measuring Devices

The following tools were utilized in this study to investigate the impact of nanoscale silver particles on bacteria:

3.7.1 Ultraviolet-visible spectroscopy

The optical characterization of nanoparticles gives information about physical properties such as transmittance, absorbance, and band gap energy.

The samples were examined by a UV-Visible (2601) double-beam spectrophotometer at Science College, the University of Anbar as shown in Figure 3.5. The colloidal samples of Ag NPs with different concentrations and different exposure times are placed in a quartz cell at 1 cm depth. The optical absorbance spectrum of the Ag NPs was determined by using a UV-Visible spectrophotometer (the wavelength range between 200-700 nm) was used to study the absorbance spectrum.

Figure 3.5 UV-Visible spectrophotometer

3.7.2 X-ray diffraction measurements (XRD)

Using XRD methods, the structural characteristics of Ag NPS were studied. It is a method for measuring the structural characteristics of crystalline phases existing in materials without causing any touch or damage to them. XRD device records the intensity as a function of diffraction angles (Bragg's angle) under the conditions of a power diffraction system with the target (Cu-K radiation), wavelength (=1.5406 Å), voltage (V=40 kV), current (I=40 mA), (step=0.0260), and diffraction angles (2θ). The structural properties and phase analysis have been examined in this study by a XRD device (Figure 3.6).

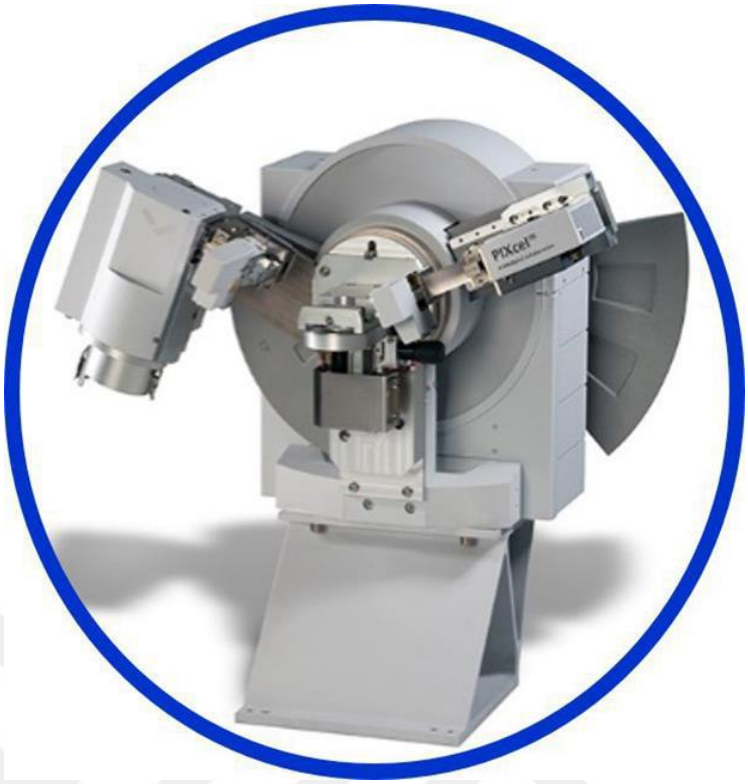

Figure 3.6 X-ray diffractometer

3.7.3 Field emission scanning electron microscope (FESEM)

To investigate the morphology and size of particles at very high magnifications, a FESEM (ZEISS SIGMA VP) (Figure 3.7) apparatus made in the USA was utilized to quantify the features of surface morphology (shape and particle size) for all samples of Ag NPs. During the examination of the FESEM, the electron beam has energies between 10 and 30 kV.

Figure 3.7 Field emission scanning electron microscopy system

3.7.4 Dynamic light scattering (DLS) and zeta potential

The Zetasizer Nano ZS is a high-performance two-angle particle, zeta-potential, and molecular size analyzer for the enhanced detection of aggregates and minute particles. Samples may be evaluated at extremely low or high concentrations using dynamic light scattering and "NIBS" optics. Sizes between 0.3 nm and 10 um may be measured. Measurements of the zeta-potential may be done between 3.8 nm and 100 um. By connecting to an SEC or an FFF system utilizing the flow mode option, the device may be used as a detector for the size of proteins or nanoparticles. Automatic examination of the effects of changes in conductivity, pH, or any additive is possible with the MPT-2 Autotitrator. A range of single-use and reusable cells are available to optimize the measurement in terms of sample quantity, concentration, and flow measurement (Figure 3.8).

Figure 3.8 Dynamic light scattering (DLS) and zeta potential system

3.7.5 Inductively coupled plasma mass spectrometry (ICP-MS)

The inductively coupled plasma mass spectrometry (ICP-MS) instrument (PerkinElmer Optima 7300DV/USA) was used to determine the amounts of MNPs in liquids, as shown in Figure 3.9. ICP-MS was created to combine the simplicity of sample introduction and speedy analysis offered by ICP (Inductively Coupled Plasma) technology with the precision and extremely low detection limits offered by a mass spectrometer, which is limited in its ability to perform as many scans per second as an ICP-MS device. ICP-MS is used for the quantitative and qualitative analysis of components in solution or liquid samples. Multi-element analysis, which is often carried out at the part per trillion level, may be tracked by the equipment. ICP-MS is a method that combines a mass spectrometer with a high-temperature inductively coupled plasma source. In general, the argon gas was heated to create a plasma flame, which converted the atoms of the sample's elements to ions. The mass spectrometer is then used to separate and detect these ions. Finally, the

ion concentrations of the samples are estimated by the use of multi-element reference standards that have been calibrated.

Figure 3.9 ICP-MS (PerkinElmer Optima 7300DV/USA)

4. RESULTS AND DISCUSSION

This chapter focuses on studying the analysis formation and syntheses mechanism of Ag NPs and characterizing their properties by different measurements, with an interest in the study of different variables during synthesis, such as the concentration of material and the exposure time to cold plasma. Finally, we will select the better results of synthesized Ag NPs, and discussion their biological activity against (Gram-positive and Gram-negative) pathogenic bacteria isolated from clinical samples, as well as study the cytotoxicity of synthesized nanoparticles.

4.1 Characterization of Silver Colloidal

Some of the physical and chemical properties of silver are changed when the silver substance is reduced to nanoparticles and dissolved in magnetized or deionized water. Colloidal silver may be created once the nanosilver particles are suspended. It was found that the color of colloidal silver tended to be yellow due to scattering effects. It was found that the colloidal color shifted from dazzling yellow to darker yellow and light green as the nanosilver's density increased (Figure 4.1).

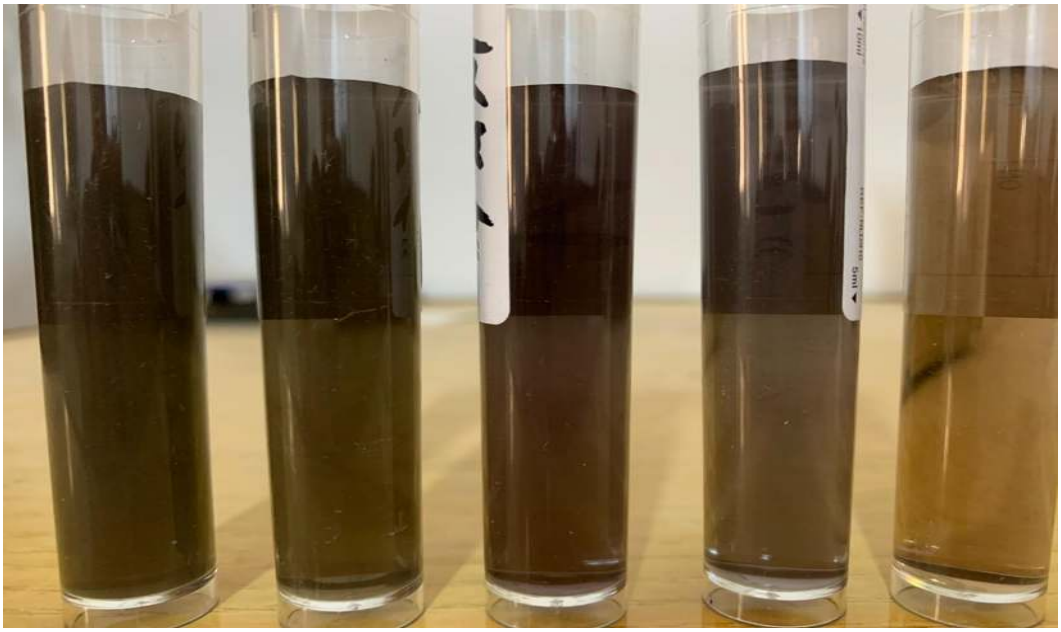

Figure 4.1 Solution colors at different concentrations (0.6, 0.8, 1, 1.2, and 1.4 mM).

This means that when the concentration of silver nanoparticles in the solution increases, the color of the colloidal solution will change. This fact was investigated experimentally using the relationship between absorbance peaks and nanoparticle concentration.

4.2 Absorption Spectra of Ag NPs

The formation of nanoparticles absorption spectrum was determined using UV–VIS spectra under the wavelength range of 200-1.000 nm. A sampling of $AgNO_3$ powder was done of plasma exposure for 5 min during the syntheses of Ag Nps, with different concentrations (0.6, 0.8, 1, 1.2, and 1.4 mM).

Ag NP absorbance spectra are shown in Figure 4.2 and Table 4.1 for various concentrations (0.6, 0.8, 1, 1.2, and 1.4 mM). The absorbance peaks in the visible region are the characteristic metals NPs formation, while confinement in the nanoscale was proved by a Redshift in plasmon absorption peak with an increase of concentration and an increase in the intensity with an increase of concentration.

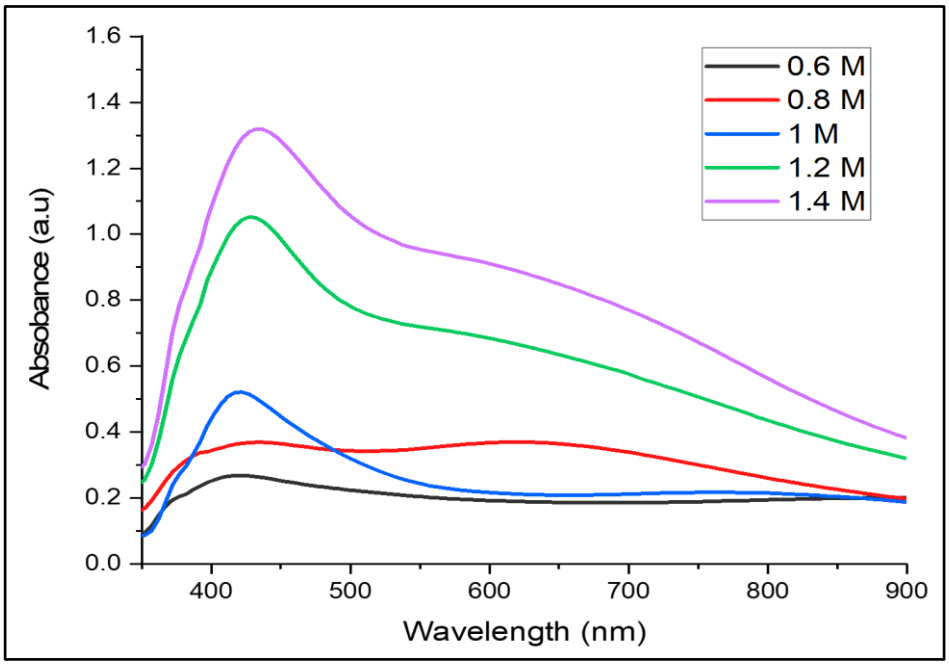

Figure 4.2 Absorbance of Ag NPs for different concentration

Table 4.1 Values of absorption for Ag NPs

Concentration (mM)	Relative intensity (abs) (a.u)	$\lambda\, max$ (nm)
0.6	0.26	416
0.8	0.33	417
1	0.52	421
1.2	1.04	428
1.4	1.3	433

Gustav Mie's theory explains the nanoscale silver particle-induced absorption phenomenon. Depending on the size and form of the nanoparticles, the colloid color is discovered. The color of the colloidal solution containing varied quantities of nanosilver changed from brilliant yellow to darker yellow to light green depending on the quantity of nanosilver and its form as illustrated in Figure 4.1. Moreover, it was found that the absorption peaks varied in height between 0.26 and 0.28 nm, and they defined a surface Plasmon band in the 420–430 nm range that is indicated by nanosilver. The absorption spectra are produced by the interactions of a free electron present in nanoscale silver particles with incoming light, while the peak position (SPR) is 420 nm.

4.3 X-Ray Diffraction (XRD) Analysis

Figure 4.3 and Figure 4.4 shows the XRD pattern of the prepared Ag nanoparticles by using a plasma jet at different concentrations (0.6, 0.8, 1, 1.2, 1.4 mM) of silver nitrate ($AgNO_3$) with plasma exposure time is (4) minutes on substrate silicon.

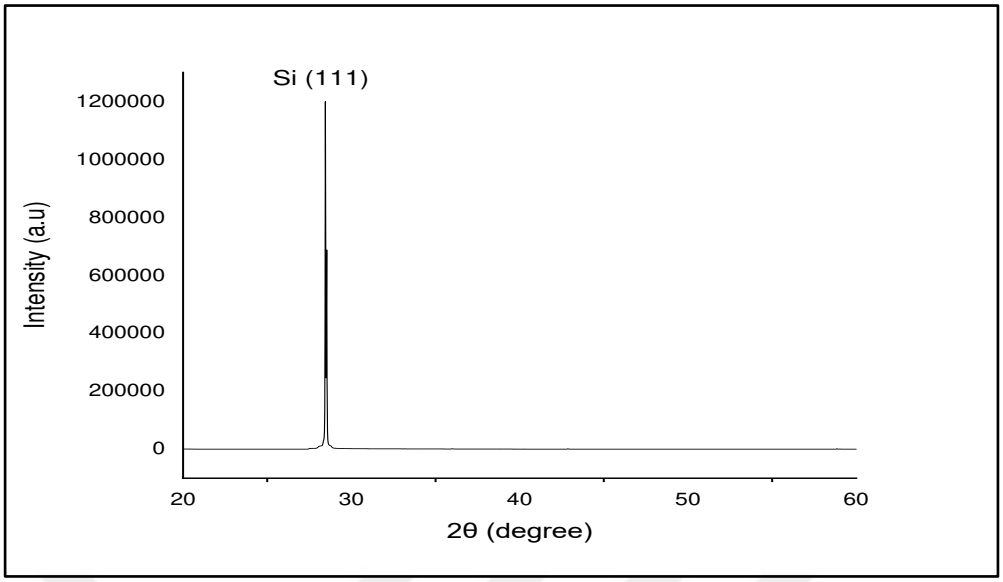

Figure 4.3 XRD pattern of silicon

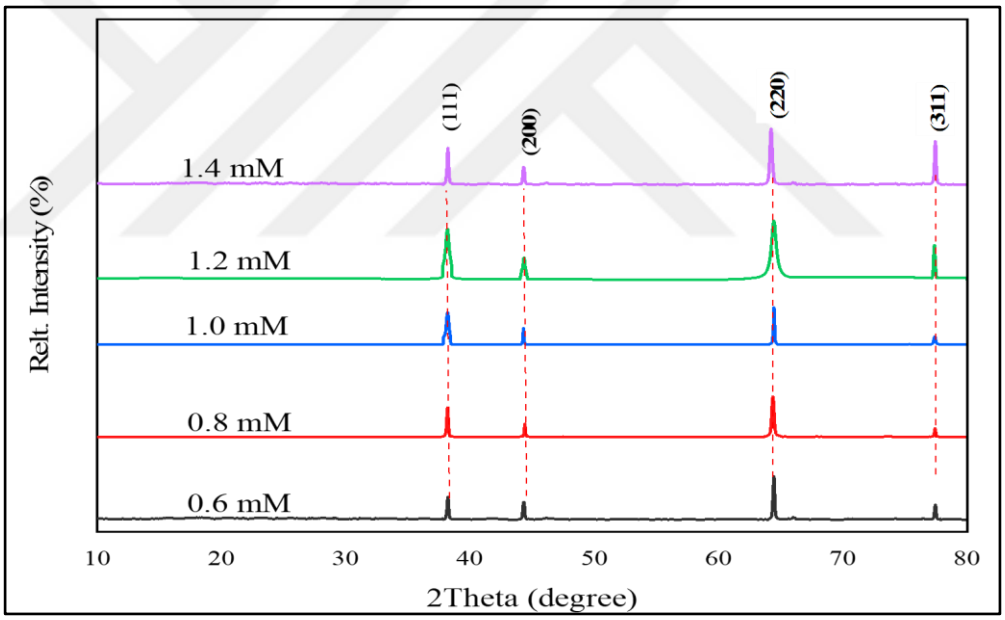

Figure 4.4 XRD pattern of silver nanoparticles at different concentrations

By comparing the results with the standard cards (JCPDS), it was found that the membrane has a cubic structure, with the appearance of crystalline levels (111), (200), (220), and (311) at the boundary angles 38.1, 44.27, 64.4, 77.4, respectively. These obtained peaks agreed well with the cubic structure of the space group (JCPDS reference code: 04-0783), referring that the crystalline growth of Ag nanostructure at different concentrations being in the same cubic phase. Observed that the increase in silver nitrate

concentration led to a high crystallinity degree of obtained silver nanoparticles. The broad peaks indicate the formation of silver nanoparticles. As for the silicon base, the apparent diffraction peak was drawn at an angle of 28.4 due to the high intensity to interpret the other diffraction peaks. At a higher concentration (1.4 mM), observed that an increase in the peak intensity indicates high crystallization of the silver nitrate phase, which is attributed to the high concentration of $AgNO_3$ in the starting solution. Table 4.2 presents the XRD calculations of silver nanoparticles at different concentrations with time (4 min).

Table 4.2 XRD calculations of Ag nanoparticles at different concentrations

Concentration (mM)	2θ (deg)	FWHM (Deg)	Crystalline size (nm)	dhkl (°A) Practical	(hkl)
0.6	**38.1**	0.149	56.38	2.36	(111)
	44.27	0.20	42.86	2.04	(200)
	64.42	0.155	60.5	1.44	(220)
	77.47	0.17	59.88	1.23	(311)
0.8	**38.1**	0.152	55.27	2.36	(111)
	44.27	0.12	95.25	2.04	(200)
	64.42	0.226	41.52	1.44	(220)
	77.47	0.11	92.54	1.23	(311)
1	**38.1**	0.309	27.18	2.36	(111)
	44.27	0.146	90.24	2.04	(200)
	64.42	0.117	80.21	1.44	(220)
	77.47	0.195	52.20	1.23	(311)
1.2	**38.1**	0.43	19.53	2.36	(111)
	44.27	0.28	30.61	2.04	(200)
	64.42	0.56	16.76	1.44	(220)
	77.47	0.147	69.25	1.23	(311)
1.4	**38.1**	0.153	54.91	2.36	(111)
	44.27	0.19	45.12	2.04	(200)
	64.42	0.232	40.45	1.44	(220)
	77.47	0.16	63.62	1.23	(311)

4.4 FE-SEM Measurement of Ag Nanoparticles

Figure 4.5 (A, B, C, D, E) shows the FESEM microscopic images of Ag nanoparticles of different concentrations of $AgNO_3$ (0.6, 0.8, 1, 1.2, and 1.4 mM) at plasma exposure time (4 min). The FESEM images demonstrated that the particle size of prepared Ag nanoparticles decreased with an increase in the $AgNO_3$ concentration, the average particle sizes are 63.8, 45.13, 44.16, 38.11, and 26.05 nm at the $AgNO_3$ concentration (0.6, 0.8,

1, 1.2, 1.4 mM) respectively with almost spherical shape. We observed that there was a small amount of non-spherical silver nanoparticles which are usually detected in plasma-assisted synthesis technique.

The concentration of the ionic silver precursor steadily decreased as the concentration of $AgNO_3$ grew, but the number of silver nanoparticles generated increased. The anisotropic growth of the produced silver nanoparticles is preferred to the nucleation of new nanoparticles when the concentration of the silver precursor is low (De Vos *et al.* 2017).

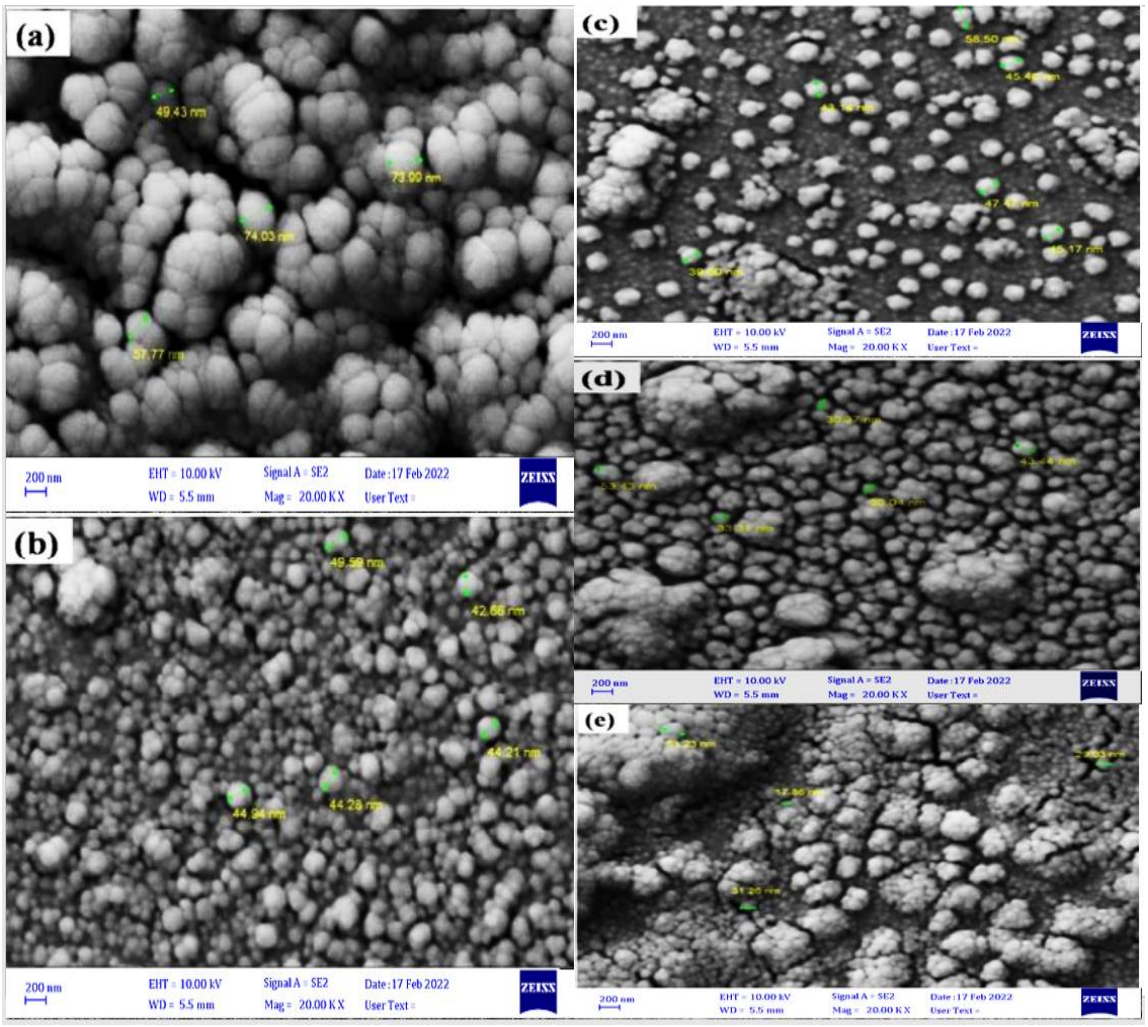

Figure 4.5 The microscopic images of Ag nanoparticles of different concentrations of $AgNO_3$ (a) 0.6 mM, (b) 0.8 mM, (c) 1 mM, (d) 1.2, (e) 1.4 mM, with time (4 min)

4.5 DLS Analysis of Ag NPs

Most often, semi-elastic light scattering is associated with dynamic light scattering. DLS is used to assess the dispersion and size of nanoparticles because it controls the size distribution and selective aggregation of nanoparticles (Iqbal *et al.* 2020).

The silver nitrate nanoparticle solution obtained after 4 min plasma discharge for different initial $AgNO_3$ concentrations (0.6, 0.8, 1, 1.2, and 1.4 mM) is analyzed by DLS for particle size determination. The particle size measurement results are presented in Figure 4.6, Figure 4.7, Figure 4.8, Figure 4.9, and Figure 4.10, as a number-based particle size distribution (PSD). This is particularly necessary to detect whether or not the nanoparticles are monodispersive. The particles produced by the plasma flow procedure with a concentration of 0.6 mM over 4 min had a diameter of 54.96 nm for 100% of the particles, according to the measurements of the particle diameter. It scatters between 34 and 147 nm. The size distribution of the particles at the concentration of 0.8 mM is shown in Figure 4.7, and the results of the DLS demonstrate that 100% of the particles had a diameter of 42.81 nm in the range of 30-127 nm. Figure 4.8 presented the size distribution of the particles of the concentration (1 mM), indicating that 100% of the particles have a diameter of 91.48 nm, and that particle diameter values are dispersed between 45-220 nm. The DLS results in Figure 4.9 show the size distribution of the particles of the concentration (1.2 mM), indicating that 100% of the particles have a diameter of 62.86 nm, and that particle diameter values are dispersed between 34-200 nm. Last but not least, the DLS findings in Figure 4.10 showed the size distribution of the particles at the concentration (1.4 mM), showing that 100% of the particles have a diameter of 87.25 nm and that particle diameter values are scattered between 45-200 nm, as given in Table 4.3. It is important to be aware that the polydispersity index (PDI) for DLS is computed by $(\text{width/mean})^2$ for each peak and generally illustrates the intensity of light dispersed by different percentages of particles of different sizes. Whereas values of 0.1-0.4 and (>0.4) are thought to be moderately and extremely polydisperse, respectively, PDI of 0.1 is thought to be very monodisperse (Bhattacharjee 2016). However, according to Andronescu and Grumezescu (2017), monodisperse nanoparticles are those having a polydispersity value of less than 0.4.

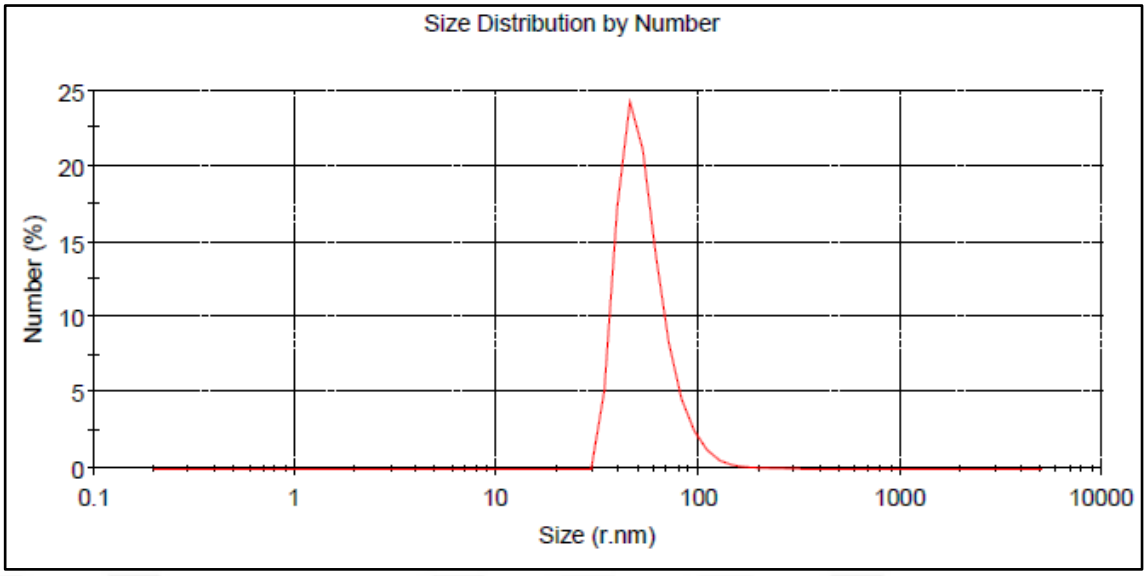

Figure 4.6 The size distribution of the particles of (number of individual particles versus aggregate sizes) prepared with concentration (0.6 mM)

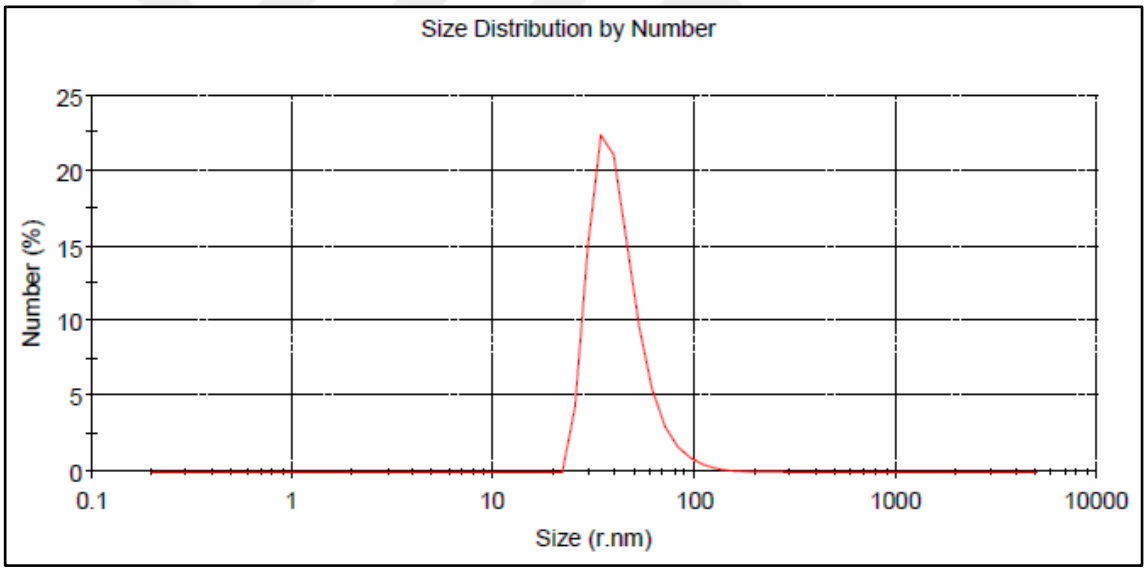

Figure 4.7 The size distribution of the particles of (number of individual particles versus aggregate sizes) prepared with concentration (0.8 mM)

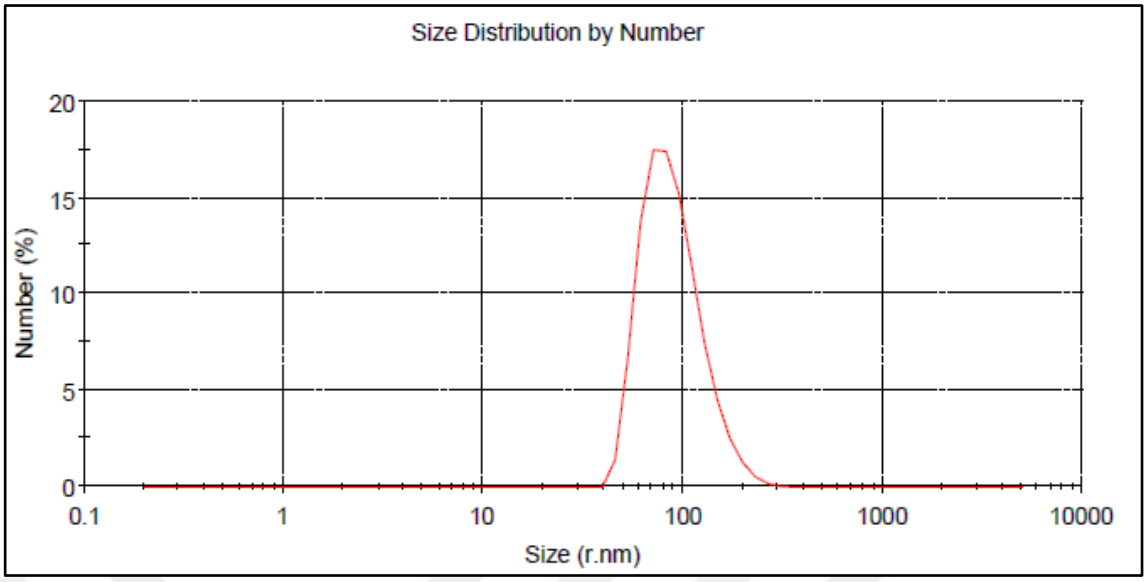

Figure 4.8 The size distribution of the particles of (number of individual particles versus aggregate sizes) prepared with concentration (1 mM)

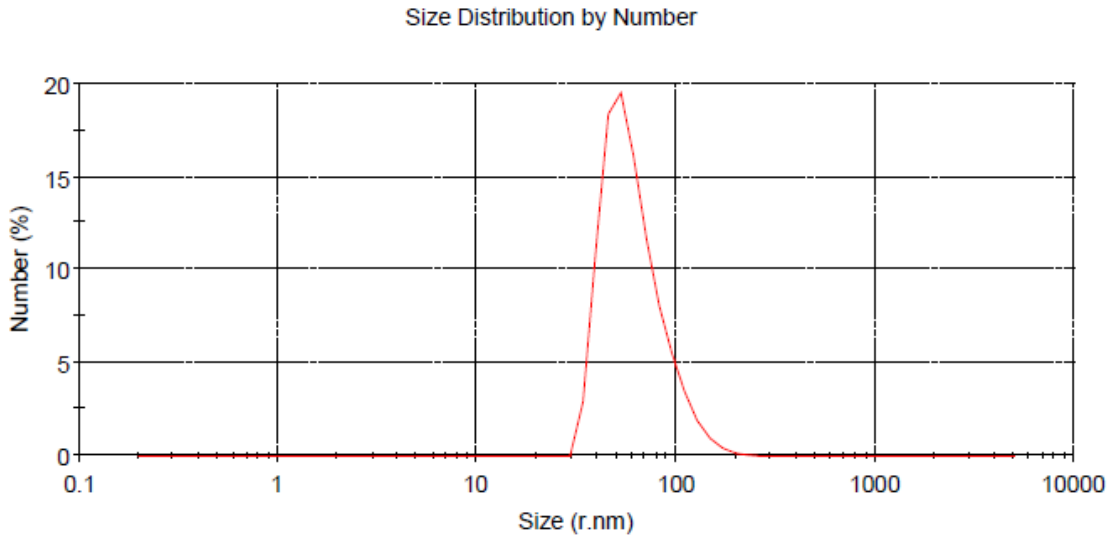

Figure 4.9 The size distribution of the particles of (number of individual particles versus aggregate sizes) prepared with concentration (1.2 mM)

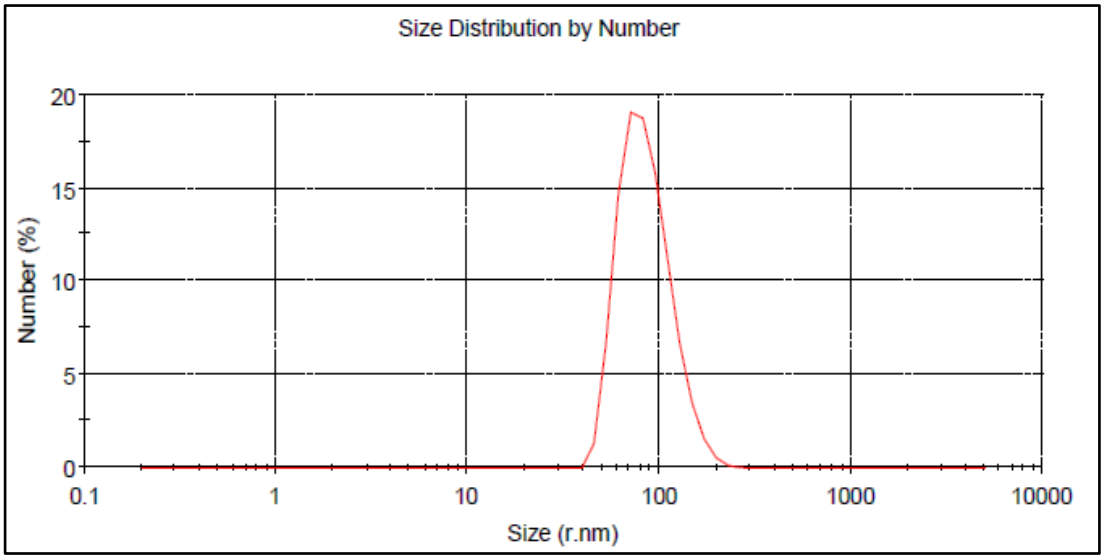

Figure 4.10 The size distribution of the particles of (number of individual particles versus aggregate sizes) prepared with concentration (1.4 mM)

Table 4.3 The results obtained by DLS size measurements performed on $AgNO_3$ solutions with different concentrations

Concentration (mM)	Peaks	Number-based size		Particle distribution range(nm)	Pdi
		(N %)	(nm)		
0.6	1	100%	54.96	34-147	0.455
0.8	1	100%	42.81	30-127	0.476
1	1	100%	91.48	45-220	0.178
1.2	1	100%	62.86	34-200	0.242
1.4	1	100%	87.25	45-200	0.209

4.6 Zeta Potential Analysis

Zeta potential measurements may also be used to evaluate the stability of colloidal particles. Absolute values are used to depict the electrical charge on the surface of the particle. When a substance's zeta potential falls between 0 and 10 mV, 10 and 20 mV, 20 and 30 mV, and +30 mV, it is said to be very unstable, reasonably stable, moderately stable, or highly stable (Bhattacharjee 2016).

In this study, the results of Ag nanoparticle solution obtained after 4 min plasma discharge for different initial $AgNO_3$ concentrations (0.6, 0.8, 1, 1.2, and 1.4 mM) nanoparticle solution are analyzed by zeta potential, after plasma discharge for different concentrations

as an initial step, as shown in Figure 4.11, Figure 4.12, Figure 4.13, Figure 4.14 and Figure 4.15. The Z-potential value of the concentration 0.6 mM was found 27.2 mV in Figure 4.11, while the Z-potential with a concentration of 0.8 mM was -16 mV as illustrated in Figure 4.12. Also, the Z-potential value of concentration 1 mM was found to be -21.3 mV, as shown in Figure 4.13. Additionally, the Z-potential value of concentration 1.2 mM was found to be 65.5 mV, as shown in Figure 4.14. Finally, the Z-potential value of the concentration 1.4 mM was found at 40.2 mV in Figure 4.15, and that is due to the high aggregation that occurs in this concentration (Instruments 2011).

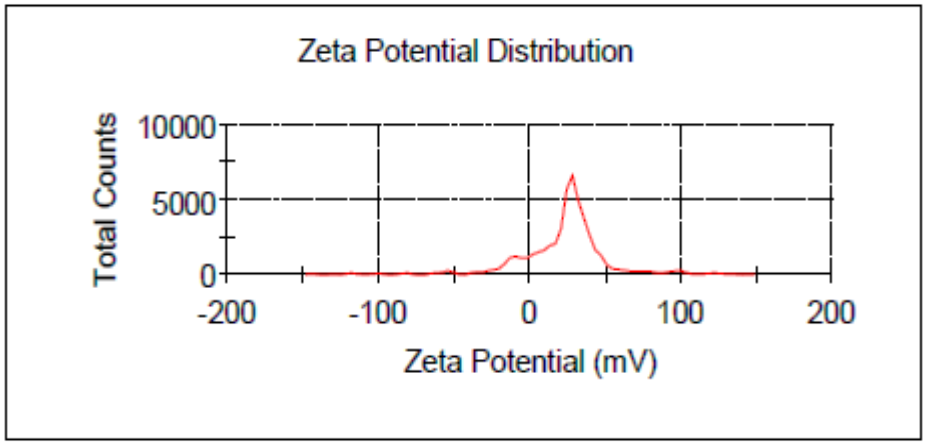

Figure 4.11 Zeta potential measurements prepared with concentration (0.6 mM)

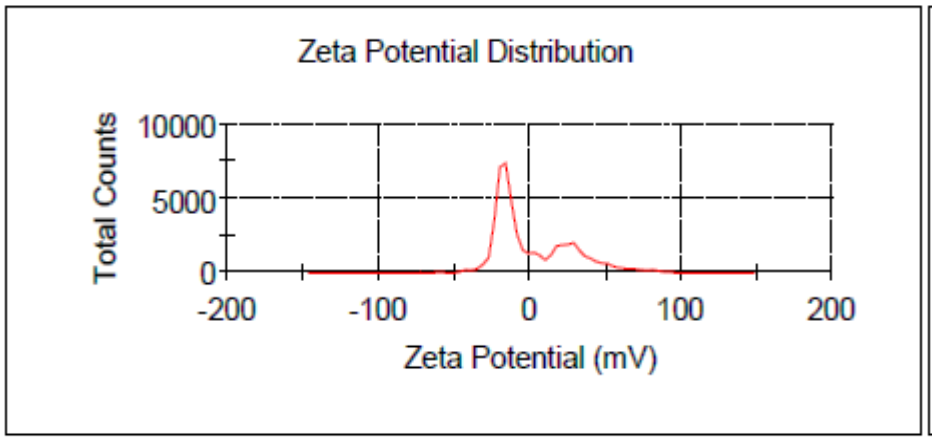

Figure 4.12 Zeta potential measurements prepared with concentration (0.8 mM)

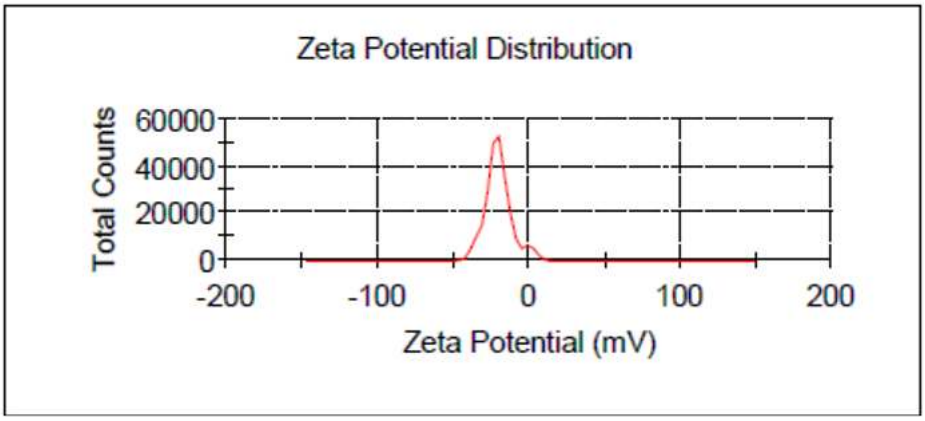

Figure 4.13 Zeta potential measurements prepared with concentration (1 mM)

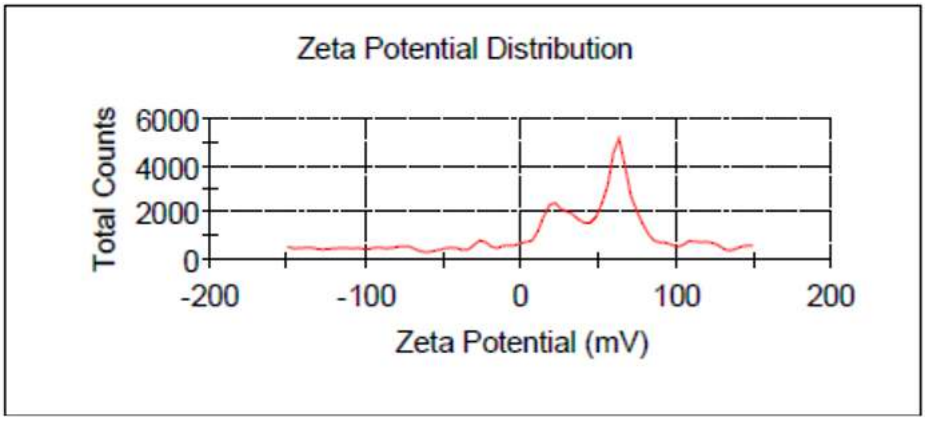

Figure 4.14 Zeta potential measurements prepared with concentration (1.2 mM)

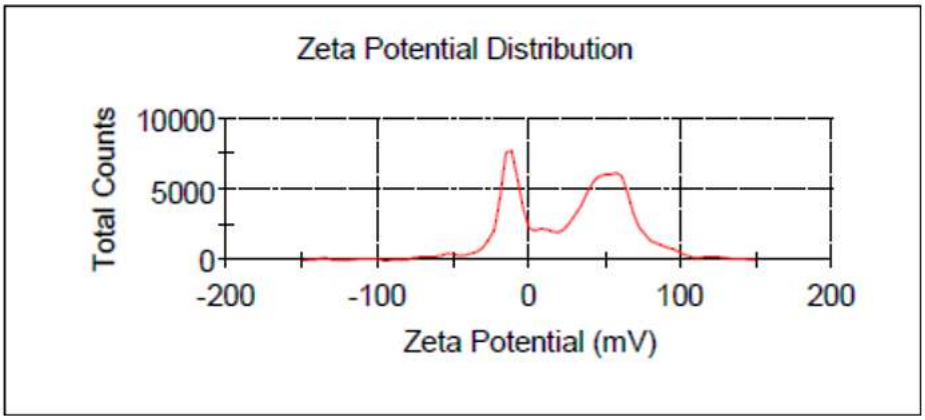

Figure 4.15 Zeta potential measurements prepared with concentration (1.4 mM)

It should be emphasized that ZP only deals with surface potential and never measures charge or charge density. Hence, just ZP's size matters, and its related positive or negative result is not reliable.

Moreover, other variables may convert it from +ve to -ve and vice versa (for example, pH, which is important for nanoformulations). If the dominating ions in the EDL up to the sliding plane are comparable (positive/negative) to the surface of the particle itself, then ZP merely gives suggestive evidence of the nature of the surface charge (positive/negative) (Bhattacharjee 2016). However, in our case, the pH of the solution and the concentration of the metal particles, such as Au, Ag, Ni, Cr, and Fe particles, are what determine the charge on their surface, which is typically negative. These metal particles are classified as hydrophobic colloids and have negative Z-potential values. Due to their negative surface charges, which prevent particle aggregation, these particles display a high repulsive force. The particles' repelling forces caused by the negative surface charge prevent the particles from coagulating. The fact that all of the Z-potential values obtained for all concentrations were low can be attributed to the fact that, while ZP does give hints about colloid stability, it does not capture the full picture, by the most widely accepted DLVO, which claims that (Theory colloid stability depends on the sum of van der Waals attractive forces and electrostatic repulsive forces due to the EDL) (Lee *et al.* 2015).

From the above-mentioned results, Z-potential is measured for the better concentration selected, which is 1 mM≈-19.8 µg/mL NPs.

4.7 ICP-MS Spectroscopy Analysis of Ag NPs

The extra contaminants in the liquid were located using an inductively coupled plasma mass spectrometry as well as the dissolved metal components of $AgNO_3$. ICP-MS is an analytical method used to qualitatively and quantitatively assess components in solution or liquid samples. ICP-MS analysis offers data on elemental abundance at extremely high precision (parts per billion), and is especially useful for measuring heavy elements (Bulska and Ruszczyńska 2017).

To complete the analysis of the properties of silver in our research, we quantitatively assess the types and quantities of metal impurities contained in manufactured samples. The exposure time of the plasma jet made sure that the silver nitrate and water were thoroughly destroyed.

Although the maximum percentage was at concentration, the data revealed that the concentration of Silver rose as $AgNO_3$ concentration increased (Figure 4.16). Also, the samples' ICP-MS analyses showed that the approach successfully ionized and detected the metal impurities including Al, Se, Te, Ni, Zn, and P that are often found in precursors to silver nitrate. It was challenging to determine whether the metal was discovered to be in a free form in the solution or its oxide because of the plasma jet treatment that was done to the solution to completely disintegrate it and produce the nanoparticles. Due to this, only H and He, Ar, N, and O, which are abundant in plasma and air and cannot be ionized in argon plasma, N and O that cannot be ionized by plasma, and H and He that are below the mass range of the mass spectrometer cannot be measured by ICP-MS (Pröfrock and Prange 2012).

Sample No.	Element (ppb)										
	Nb	Mo	Ru	Rh	Pd	Ag	Cd	In	Sn	Sb	Te
0.6	<0.1	12.42	<0.1	<0.1	<0.1	748557.36	0.42	<0.1	8.39	0.79	147.06
0.8	<0.1	18.88	<0.1	<0.1	<0.1	391725.17	0.06	<0.1	1.66	0.58	0.00
1.0	<0.1	18.13	<0.1	<0.1	<0.1	2176512.81	0.24	<0.1	1.54	1.83	264.71
1.2	<0.1	19.36	<0.1	<0.1	<0.1	1691218.17	0.29	<0.1	8.80	0.36	117.65
1.4	<0.1	17.25	<0.1	<0.1	<0.1	1642063.22	0.25	<0.1	9.91	0.38	147.06

Figure 4.16 Elements concentration of Ag NPs samples with an exposure time of cold plasma jet 4 min as a function of different concentrations (0.6, 0.8, 1, 1.2, and 1.4 mM)

4.8 Antibacterial Activity of Ag NPs

The antibacterial activity of the synthesized Ag NPs against Both Gram-negative and Gram-positive bacteria were investigated by the Well Diffusion Method (zone of

inhibition, ZOI) (Ramesh *et al.* 2012). Briefly, the pure colonies of the types of pathogenic bacteria were grown in an MHB medium overnight at 37°C. Spreading a known volume of overnight culture fresh pathogens solution over the surface of the MH agar was spread uniformly, and the NPs solution is filled into a-holes or wells created on the agar medium with concentrations (0.6, 0.8, 1, 1.2, and1.4 mM) with one well of precursor solution Ag NPs as (positive control). All plates were incubated at 37°C for 24 h to check the zone of inhibition (ZOI). After incubation, the zones of inhibition were measured by measuring the diameter of the zone around each well and expressed in millimeters (mm). Moreover, the Ag NPs exhibited superior antibacterial activity in terms of ZOIs against Gram-positive and Gram-negative bacteria at concentration levels (1 mM) only; they presented a clear inhibitory efficacy compared to other concentrations, as shown in Figure 4.17.

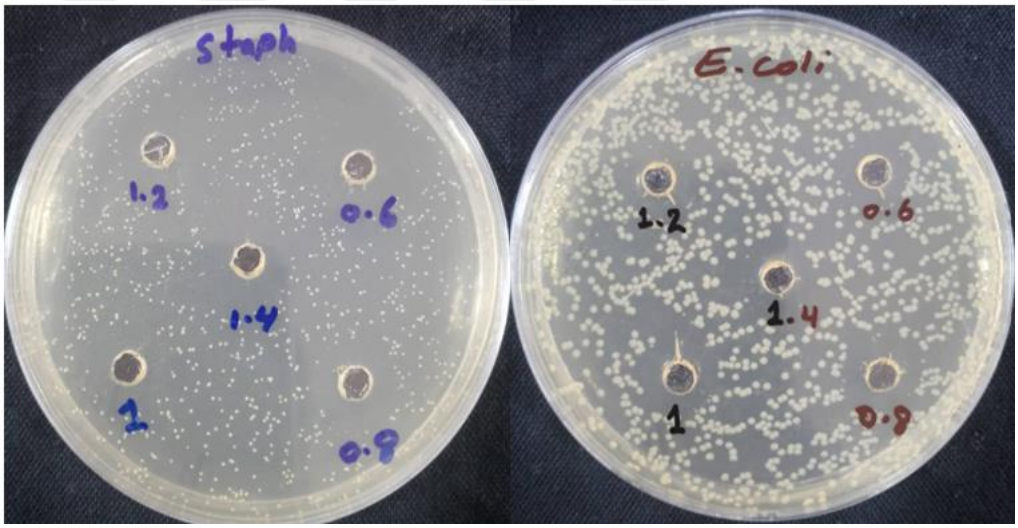

Figure 4.17 The antibacterial activity of Ag NPs against Gram-positive bacteria (*S. aureus*) and Gram-negative (*E. coli*) with the concentrations 0.6, 0.8, 1, 1.2 and 1.4 mM

Ag nanoparticles' antibacterial activity is influenced by their size and shape. Ag NPs with a small size ensure that a significant amount of their surface area is in contact with bacterial effluent, and as a result, have a greater antibacterial effect because they expose more of the bacterial membrane to the surface. It is anticipated that having such a vast contact area will increase the degree of bacterial clearance. As a result, they attach to the cell membrane of bacteria and interact with their cell walls, altering the membrane

potential in the process to alter permeability. Yet being little in and of itself is not the aim. The dwellers of bactericidal materials are very interested in the synthesis and characterization of nanoscaled materials in terms of their physicochemical characteristics (Pal *et al.* 2007). The inhibition values provided in Table 4.4 in the findings further revealed that Gram-positive bacteria were found to be more vulnerable to Ag NPs than Gram-negative bacteria. This may be because both bacteria's cell walls differ in their chemical makeup and structure, as well as in how susceptible they are to metal oxide nanoparticles. Gram-negative bacteria have phospholipids, lipoproteins, and lipopolysaccharides as part of their cell walls. In contrast, the cell walls of Gram-positive bacteria have big holes and a thick covering of peptidoglycan and teichoic acid. Moreover, Gram-positive bacteria have a higher surface negative charge than Gram-negative bacteria, which attracts nanoparticles more effectively. Due to their tiny size and ability to spread and break bacterial cell walls at low temperatures, nanoparticles can kill germs (Khan *et al.* 2021).

Table 4.4 The results of ZOI by well diffusion method of Ag NPs, against *Escherichia coli* and *Staphylococcus aureus*

Concentration (Mm)	***Staphylococcus aureus***	***Escherichia coli***
0.6	15.43427	12.56828
0.8	14.32116	12.91816
1	15.01592	13.73081
1.2	14.1871	13.68434
1.4	15.47548	14.32116

5. CONCLUSIONS AND RECOMMENDATIONS

5.1 Conclusions

- In the current work, silver nanoparticles are synthesized using non-thermal atmospheric plasma in an easy and fast way and this material is used for medical and biological applications.
- The absorption spectrum peaks analyzed by UV/VIS spectroscopy are around 390-420 nm for silver nanoparticles these are the characteristics of noble metal nanoparticles which are called surface plasmon resonance. The maximum absorbance was found at a concentration of 1.4 mM with an exposure time of 4 min of plasma.
- The presence of silver nanoparticles is confirmed by X-ray diffraction. It is found to have four strong peaks of 2θ at 38.1°, and another peak appears at 44.27°, 64.42° and 77.47° for silver nanoparticles. The peaks became more clear and had high crystallization with a concentration of 1.4 mM with an exposure time of 4 min of plasma.
- The FESEM demonstrated that the particle size of prepared Ag nanoparticles increased with the increase of $AgNO_3$ concentration at plasma exposure time (4 min).
- Antibacterial activity was observed in the nanoparticles synthesized in this study against both Gram-positive bacteria (*Staphylococcus aureus*) and Gram-negative bacteria (*Escherichia coli*), so these results are very encouraging to be these NPs active on the other types of pathogenic bacteria.

5.2 Recommendations

According to the findings obtained from this research, the following topics are recommended:

- To study the influence of Ag NPs on the cancer cell lines in addition to normal cells line and note which gives better results.
- To study the influence of Ag NPs and NiNPs on other types of pathogenic bacteria.

- Studying the antifungal activity of Ag NPs and Ni NPs synthesized by the technique DC cold plasma jet.

REFERENCES

Abdul-Hassan, I. A., Abbas, A. K. and Ibrahim, I. M. 2018. Plasma characteristics of Ag and Cu metals produced by pulse laser ablation of Nd:YAG laser in air. Journal of Recent Research and Applied Studies, 18(1): 1-6.

Al-Azawi, M. T., Mohammed, C. H. and Hadi, S. M. 2018. Ag-SiO2 nanoparticales prepared by Sol-Gel methods for antibacterial effect. Iraqi Journal of Physics, 16(39): 135-151.

Alexandre, M. A., Pérez, E., Lacabanne, C., Dantras, E., Franceschi-Messant, S., Coudeyre, D. and Garrigues, J. C. 2018. Formulation of Aqueous dispersions of PEKK by a Quantitative structure property relationship approach and application to thermoplastic sizing on carbon fiberss. Advances in Materials, 7(4): 118-127.

Andronescu, E. and Grumezescu, A. M. 2017. Nanostructures for drug delivery. Elsevier, 1024 page, Amsterdam.

Ayala-Núñez, N. V., Lara Villegas, H. H., del Carmen Ixtepan Turrent, L. and Rodríguez Padilla, C. 2009. Silver nanoparticles toxicity and bactericidal effect against methicillin-resistant Staphylococcus aureus: nanoscale does matter. Nanobiotechnology, 5: 2-9.

Bhattacharjee, S. 2016. DLS and zeta potential–what they are and what they are not?. Journal of Controlled Release, 235: 337-351.

Brandenburg, R. 2017. Dielectric barrier discharges: progress on plasma sources and on the understanding of regimes and single filaments. Plasma Sources Science and Technology, 26(5): 053001.

Brooks, G. F., Carroll, K. C., Butel, J. S., Morse, S. A., Mietzner, T. A. and Jawetz, M. 2007. Adelberg's medical microbiology. Sultan Qaboos University Medical Journal, 7(3): 273.

Bulska, E. and Ruszczyńska, A. 2017. Analytical techniques for trace element determination. Physical Sciences Reviews, 2(5).

Burm, K. T. A. L. 2012. Plasma: The fourth state of matter. Plasma Chemistry and Plasma Processing, 32: 401-407.

Buzea, C., Pacheco, I. I. and Robbie, K. 2007. Nanomaterials and nanoparticles: sources and toxicity. Biointerphases, 2(4): 17-71.

Byrns, B., Wooten, D., Lindsay, A. and Shannon, S. 2012. A VHF driven coaxial atmospheric air plasma: electrical and optical characterization. Journal of Physics D: Applied Physics, 45(19): 195204.

Callen, J. D. 2006. Coulomb collisions. Fundamentals of Plasma Physics, 1-57.

Chang, J. S., Lawless, P. A. and Yamamoto, T. 1991. Corona discharge processes. IEEE Transactions on Plasma Science, 19(6): 1152-1166.

De Vos, C., Baneton, J., Witzke, M., Dille, J., Godet, S., Gordon, M. J. and Reniers, F. 2017. A comparative study of the reduction of silver and gold salts in water by a cathodic microplasma electrode. Journal of Physics D: Applied Physics, 50(10): 105206.

Deng, X. L., Nikiforov, A. Y., Vanraes, P. and Leys, C. 2013. Direct current plasma jet at atmospheric pressure operating in nitrogen and air. Journal of Applied Physics, 113(2): 023305.

Feng, Q. L., Wu, J., Chen, G. Q., Cui, F. Z., Kim, T. N. and Kim, J. O. 2000. A mechanistic study of the antibacterial effect of silver ions on Escherichia coli and Staphylococcus aureus. Journal of Biomedical Materials Research, 52(4): 662-668.

Filipponi, L., Sutherland, D. and Center, I. N. 2010. Introduction to nanoscience and nanotechnologies. NANOYOU Teachers Training Kit in Nanoscience and Nanotechnologies, 1-29.

Förster, S., Mohr, C. and Viöl, W. 2005. Investigations of an atmospheric pressure plasma jet by optical emission spectroscopy. Surface and Coatings Technology, 200(4): 827-830.

Fridman, A., Chirokov, A. and Gutsol, A. 2005. Non-thermal atmospheric pressure discharges. Journal of Physics D: Applied Physics, 38(2).

García-Alcantara, E., López-Callejas, R., Morales-Ramírez, P. R., Peña-Eguiluz, R., Fajardo-Muñoz, R., Mercado-Cabrera, A. and Rojas-Olmedo, I. A. 2013. Accelerated mice skin acute wound healing in vivo by combined treatment of argon and helium plasma needle. Archives of Medical Research, 44(3): 169-177.

Gubicza, J. 2017. Defect structure and properties of nanomaterials. Woodhead Publishing, 410 page, Cambridge.

Guozhong, C. 2004. Nanostructures and nanomaterials: synthesis, properties and applications. World Scientific, 581 page, Singapore.

Harding, S. E. and Jumel, K. 1998. Light scattering. Current Protocols in Protein Science, 11(1): 7-8.

He, S., Chen, H., Guo, Z., Wang, B., Tang, C. and Feng, Y. 2013. High-concentration silver colloid stabilized by a cationic gemini surfactant. Colloids and Surfaces A: Physicochemical and Engineering Aspects, 429: 98-105.

Heberlein, J. 2002. New approaches in thermal plasma technology. Pure and Applied Chemistry, 74(3): 327-335.

Hornyak, G. L., Moore, J. J., Tibbals, H. F. and Dutta, J. 2018. Fundamentals of nanotechnology. CRC Press, 786 page, Boca Raton.

Instruments, M. 2011. Zeta potential: An introduction in 30 minutes. Malvern, 1(2): 1-6.

Iqbal, J., Abbasi, B. A., Munir, A., Uddin, S., Kanwal, S. and Mahmood, T. 2020. Facile green synthesis approach for the production of chromium oxide nanoparticles and their different in vitro biological activities. Microscopy Research and Technique, 83(6): 706-719.

Irving, W., Boswell, T. and Ala'Aldeen, D. 2004. BIOS Instant notes in Medical Microbiology. Taylor & Francis, 364 page, Abingdon.

Jiang, N., Ji, A. and Cao, Z. 2009. Atmospheric pressure plasma jet: Effect of electrode configuration, discharge behavior, and its formation mechanism. Journal of Applied Physics, 106(1): 013308.

Kadhim Al-Ogaili, A., Ali, A. K. and Ali, T. H. 2015. Preparation of silver nanoparticles and study the optical and antibacterial properties. Engineering and Technology Journal, 33(30): 478-487.

Karmakar, S. T. 2019. Particle size distribution and zeta potential based on dynamic light scattering: Techniques to characterize stability and surface charge distribution of charged colloids. Recent Trends in Materials: Physics and Chemistry, 117-159.

Kaszuba, M., Corbett, J., Watson, F. M. and Jones, A. 2010. High-concentration zeta potential measurements using light-scattering techniques. Philosophical Transactions of the Royal Society A: Mathematical, Physical and Engineering Sciences, 368(1927): 4439-4451.

Kattumuri, V. 2006. Gold nanoparticles for biomedical applications: synthesis, characterization, in vitro and in vivo. PhD. Thesis, University of Missouri, 152 page, Missouri.

Khan, I., Saeed, K. and Khan, I. 2019. Nanoparticles: Properties, applications and toxicities. Arabian Journal of Chemistry, 12(7): 908-931.

Khan, S. A., Shahid, S., Hanif, S., Almoallim, H. S., Alharbi, S. A. and Sellami, H. 2021. Green synthesis of chromium oxide nanoparticles for antibacterial, antioxidant anticancer, and biocompatibility activities. International Journal of Molecular Sciences, 22(2): 502.

Khandel, P., Yadaw, R. K., Soni, D. K., Kanwar, L. and Shahi, S. K. 2018. Biogenesis of metal nanoparticles and their pharmacological applications: present status and application prospects. Journal of Nanostructure in Chemistry, 8: 217-254.

Khanna, V. K. 2016. Integrated nanoelectronics. Nanoscience and Technology, 10: 978-81.

Kim, H. H. and Ogata, A. 2011. Gas-to-particle conversion in surface discharge nonthermal plasmas and its implications for atmospheric chemistry. Sensors, 11(3): 2992-3003.

Kim, S. H., Lee, H. S., Ryu, D. S., Choi, S. J. and Lee, D. S. 2011. Antibacterial activity of silver-nanoparticles against Staphylococcus aureus and Escherichia coli. Microbiology and Biotechnology Letters, 39(1): 77-85.

Kogelschatz, U. 2003. Dielectric-barrier discharges: their history, discharge physics, and industrial applications. Plasma Chemistry and Plasma Processing, 23(1): 1-46.

Kondeti, V. S. K., Gangal, U., Yatom, S. and Bruggeman, P. J. 2017. Ag+ reduction and silver nanoparticle synthesis at the plasma–liquid interface by an RF driven atmospheric pressure plasma jet: Mechanisms and the effect of surfactant. Journal of Vacuum Science & Technology A: Vacuum, Surfaces, and Films, 35(6): 061302.

Koole, R., Groeneveld, E., Vanmaekelbergh, D., Meijerink, A. and de Mello Donegá, C. 2014. Size effects on semiconductor nanoparticles. Nanoparticles: Workhorses of Nanoscience, 13-51.

Lee, H., Chung, M., Ahn, H. G., Kim, S. J., Park, Y. K. and Jung, S. C. 2015. Effect of the surfactant on size of nickel nanoparticles generated by liquid-phase plasma method. International Journal of Precision Engineering and Manufacturing, 16: 1305-1310.

Lehn, J. M. 1993. Supramolecular chemistry—Molecular information and the design of supramolecular materials. Macromolecular Symposia, 69(1): 1-17.

Liau, S. Y., Read, D. C., Pugh, W. J., Furr, J. R. and Russell, A. D. 1997. Interaction of silver nitrate with readily identifiable groups: relationship to the antibacterialaction of silver ions. Letters in Applied Microbiology, 25(4): 279-283.

Lide, D. R. 2004. CRC handbook of chemistry and physics. CRC Press, 2712 page, Boca Raton.

Mackie, T. J. and McCartney, J. E. 1989. Microbial infections. Longman, 236-245.

Mahmood, M. A. 2012. The antibacterial effect of silver nanoparticles on some bacterial pathogens. Iraqi Journal of Physics, 10(18): 56-61.

Mahon, C. R. and Manuselis, G. 1995. Laboratory workbook in diagnostic microbiology. Saunders Company, 1088 page, Tokyo.

Maria, L., Santos, A. L., Oliveira, P. C., Valle, A. S., Barud, H. S., Messaddeq, Y. and Ribeiro, S. J. 2010. Preparation and antibacterial activity of silver nanoparticles impregnated in bacterial cellulose. Polimeros, 20: 72-77.

Morones, J. R., Elechiguerra, J. L., Camacho, A., Holt, K., Kouri, J. B., Ramírez, J. T. and Yacaman, M. J. 2005. The bactericidal effect of silver nanoparticles. Nanotechnology, 16(10): 2346.

Nehra, V., Kumar, A. and Dwivedi, H. K. 2008. Atmospheric non-thermal plasma sources. International Journal of Engineering, 2(1): 53-68.

Nejati, M., Rostami, M., Mirzaei, H., Rahimi-Nasrabadi, M., Vosoughifar, M., Nasab, A. S. and Ganjali, M. R. 2022. Green methods for the preparation of MgO nanomaterials and their drug delivery, anti-cancer and anti-bacterial potentials: A review. Inorganic Chemistry Communications, 136: 109107.

Ngô, C. & Van de Voorde, M. H. 2014. Nanomaterials: doing more with less. Nanotechnology in a Nutshell: From Simple to Complex Systems, 55-70.

Noori, A. M. 2017. Preparation of Ag nanoparticles via pulsed laser ablation in liquid for biological applications. Iraqi Journal of Physics, 15(34): 162-170.

Oberman, C. 1965. Hydromagnetic stability theory. In Lectures Presented at the Trieste Seminar on Plasma Physics, 137.

Pal, S., Tak, Y. K. and Song, J. M. 2007. Does the antibacterial activity of silver nanoparticles depend on the shape of the nanoparticle? A study of the gram-negative bacterium Escherichia coli. Applied and Environmental Microbiology, 73(6): 1712-1720.

Pekárek, S. 2003. Non-thermal plasma ozone generation. Acta Polytechnica, 43(6).

Penache, M. C. 2002. Study of high-pressure glow discharges generated by micro-structured electrode (MSE) arrays. PhD. Thesis, Johann Wolfgang Goethe Universität, 153 page, Frankfurt.

Pivovarov, O. A., Skiba, M. I., Makarova, A. K., Vorobyova, V. I. and Pasenko, O. O. 2017. Preparation of silver nanoparticles by contact nonequilibrium low-temperature plasma in the presence of sodium alginate. ResearchGate, (6): 82-88.

Prabhu, S. and Poulose, E. K. 2012. Silver nanoparticles: mechanism of antimicrobial action, synthesis, medical applications, and toxicity effects. International Nano Letters, 2: 1-10.

Pröfrock, D. and Prange, A. 2012. Inductively coupled plasma-mass spectrometry (ICP-MS) for quantitative analysis in environmental and life sciences: a review of challenges, solutions, and trends. Applied Spectroscopy, 66(8): 843-868.

Ramesh, C., Kumar, K. M., Senthil, M. and Ragunathan, V. 2012. Antibacterial activity of Cr2O3 nanoparticles against E. coli; reduction of chromate ions by Arachis hypogaea leaves. Archives of Applied Science Research, 4(4): 1894-1900.

Raza, M. A., Kanwal, Z., Rauf, A., Sabri, A. N., Riaz, S. and Naseem, S. 2016. Size-and shape-dependent antibacterial studies of silver nanoparticles synthesized by wet chemical routes. Nanomaterials, 6(4): 74.

Rheima, A. M., Mohammed, M. A., Jaber, S. H. and Hameed, S. A. 2019. Synthesis of silver nanoparticles using the UV-irradiation technique in an antibacterial application. Journal of Southwest Jiaotong University, 54(5).

Ridley, M. K., Hackley, V. A. and Machesky, M. L. 2006. Characterization and surface-reactivity of nanocrystalline anatase in aqueous solutions. Langmuir, 22(26): 10972-10982.

Ryan, K. J. and Ray, C. G. 2004. Sherris' medical microbiology. McGraw Hill, 4(2): 1-9.

Ryskova, L., Buchta, V. and Slezak, R. 2010. Photodynamic antimicrobial therapy. Central European Journal of Biology, 5: 400-406.

Sadeghi, B., Jamali, M., Kia, S., Amini, N. A. and Ghafari, S. 2010. Synthesis and characterization of silver nanoparticles for antibacterial activity. International Journal of Nano Dimension, 1(2): 119-124.

Scalisi, A. A., Compagnini, G., D'Urso, L. and Puglisi, O. 2004. Nonlinear optical activity in Ag–SiO2 nanocomposite thin films with different silver concentration. Applied Surface Science, 226(1): 237-241.

Schutze, A., Jeong, J. Y., Babayan, S. E., Park, J., Selwyn, G. S. and Hicks, R. F. 1998. The atmospheric-pressure plasma jet: a review and comparison to other plasma sources. IEEE Transactions on Plasma Science, 26(6): 1685-1694.

Senapati, S., Mandal, D., Ahmad, A., Khan, M. I., Sastry, M. and Kumar, R. 2004. Fungus mediated synthesis of silver nanoparticles: a novel biological approach. Indian Journal of Physics, 78: 101-105.

Shashurin, A., Keidar, M., Bronnikov, S., Jurjus, R. A. and Stepp, M. A. 2008. Living tissue under treatment of cold plasma atmospheric jet. Applied Physics Letters, 93(18): 181501.

Sherris, J. C. 1984. Medical microbiology: An introduction to infectious diseases. Elsevier Publishing Company, 991 page, Amsterdam.

Shrivastava, S., Bera, T., Roy, A., Singh, G., Ramachandrarao, P. and Dash, D. 2007. Characterization of enhanced antibacterial effects of novel silver nanoparticles. Nanotechnology, 18(22): 225103.

Šileikaitė, A., Prosyčevas, I., Puišo, J., Juraitis, A. and Guobienė, A. 2006. Analysis of silver nanoparticles produced by chemical reduction of silver salt solution. Journal of Materials Science, 12(4): 1392-1320.

Silver, S. 2003. Bacterial silver resistance: molecular biology and uses and misuses of silver compounds. FEMS Microbiology Reviews, 27(2): 341-353.

Skiba, M., Pivovarov, A., Makarova, A. and Vorobyova, V. 2018. Plasma-chemical synthesis of silver nanoparticles in the presence of citrate. Chemistry Journal of Moldova, 13(1): 7-14.

Skiba, M., Pivovarov, O., Makarova, A., Pasenko, A., Khlopytskyi, A. and Vorobyova, V. 2017. Plasma-chemical formation of silver nanodispersion in water solutions. ResearchGate, 6 (6): 59-65.

Söderström, D. 2008. Modelling and applications of the hollow cathode plasma. MSc. Thesis, Uppsala University, 79 page, Uppsala.

Takai, E., Ikawa, S., Kitano, K., Kuwabara, J. and Shiraki, K. 2013. Molecular mechanism of plasma sterilization in solution with the reduced pH method:

importance of permeation of HOO radicals into the cell membrane. Journal of Physics D: Applied Physics, 46(29): 295402.

Tang, Z. X. and Feng, B. L. 2014. MgO nanoparticles as antibacterial agent: preparation and activity. Brazilian Journal of Chemical Engineering, 31: 591-601.

Tokunaga, T., Kawakami, T., Higuchi, K., Yamamoto, Y. and Yamamoto, T. 2022. Effect of electron beam irradiation in gas atmosphere during ETEM. Micron, 158: 103289.

Ungula, J. 2015. Growth and characterization of ZnO nanoparticles by sol-gel process. MSc, Thesis, University of the Free State, 139 page, Lesotho.

Von Woedtke, T., Schmidt, A., Bekeschus, S., Wende, K. and Weltmann, K. D. 2019. Plasma medicine: A field of applied redox biology. In Vivo, 33(4): 1011-1026.

Vorobyova, V. and Skiba, M. 2021. Peach pomace extract as efficient sustainable inhibitor for carbon steel against chloride-induced corrosion. Journal of Bio-and Tribo-Corrosion, 7(1): 11.

Wei, L., Lin-Li, Z. and Xiao-Jing, Z. 2009. Grain size effect on electrical conductivity and giant magnetoresistance of bulk magnetic polycrystals. Chinese Physics Letters, 26(11): 117502.

Wilschefski, S. C. and Baxter, M. R. 2019. Inductively coupled plasma mass spectrometry: introduction to analytical aspects. The Clinical Biochemist Reviews, 40(3): 115.

Zhang, J. Z. 2009. Optical properties and spectroscopy of nanomaterials. World Scientific, 400 page, Singapore.